

REPORT DOCUMENTATION PAGE

Form Approved
201 0188

Public reporting burden for this collection of information is estimated to average 1 hour per response, including gathering and maintaining the data needed, and completing and reviewing the collection of information. Send comments regarding this burden estimate or any other aspect of this collection of information, including suggestions for reducing this burden, to Washington Headquarters Service, Paperwork Project, Washington, DC 20503-2902, and to the Office of Management and Budget, Paperwork Project, Washington, DC 20503-2902.

AFRL-SR-BL-TR-01-

sources,
t of this
efferson

1. AGENCY USE ONLY (Leave blank)		2. REPORT DATE 14 Jun 98	3. R 13 Jun 98
4. TITLE AND SUBTITLE (AASERT-95) Microwave-Optical Interactive Devices			5. FUNDING NUMBERS 61103D 3484/TS
6. AUTHOR(S) Dr. Fetterman			
7. PERFORMING ORGANIZATION NAME(S) AND ADDRESS(ES) University of California, Los Angeles 405 Hilgard Avenue Los Angeles, CA 90024-1406			8. PERFORMING ORGANIZATION REPORT NUMBER
9. SPONSORING/MONITORING AGENCY NAME(S) AND ADDRESS(ES) AFOSR/NE 801 North Randolph Street, Rm 732 Arlington, VA 22203-1977			10. SPONSORING/MONITORING AGENCY REPORT NUMBER F49620-95-1-0429
11. SUPPLEMENTARY NOTES			
12a. DISTRIBUTION AVAILABILITY STATEMENT Unlimited Distribution		12b. DISTRIBUTION CODE AIR FORCE OFFICE OF SCIENTIFIC RESEARCH (AFOSR) NOTICE OF TRANSMITTAL DTIC: THIS TECHNICAL REPORT HAS BEEN REVIEWED AND IS APPROVED FOR PUBLIC RELEASE LAW AFR 190-12. DISTRIBUTION IS UNLIMITED.	
13. ABSTRACT (Maximum 200 words) The ASSERT Program on Microwave - Optical interactions covered a wide range of actual device development. In particular we focused to a great degree on new types of detectors and high frequency optical mixers. Included are two approaches to traveling wave phototransistors that were developed with the idea that one could achieve both high power and high speed in a novel traveling wave structure. The use of polymer waveguide to bring light into the base of a heterojunction transistor was the key element.			
14. SUBJECT TERMS		20010419 043	
15. NUMBER OF PAGES		16. PRICE CODE	
17. SECURITY CLASSIFICATION OF REPORT UNCLASSIFIED	18. SECURITY CLASSIFICATION OF THIS PAGE UNCLASSIFIED	19. SECURITY CLASSIFICATION OF ABSTRACT UNCLASSIFIED	20. LIMITATION OF ABSTRACT UL



ELECTRICAL ENGINEERING DEPARTMENT
THE HENRY SAMUELI SCHOOL OF ENGINEERING
AND APPLIED SCIENCE
BOX 951594
LOS ANGELES, CALIFORNIA 90095-1594

Jan. 2, 2001

Dr. Howard Schlossberg
Air Force Office of Scientific Research
801 North Randolph Street, Room 732
Arlington VA 22203-1977

Dear Dr. Schlossberg:

I enclose the Final Technical report for the ASSERT Grant # F49620-95-1-0429. The Students supported under this program: David Scott and Daipayan Bhattacharya have been very successful and have worked for large Aerospace firms after graduation. Currently Dr. Scott has started a new company making very high speed, high power optical detectors based, in part, upon his thesis project.

The work that Dr. Bhattacharya did in high frequency mixing and ELO has found many uses in the high frequency field and efforts are currently being made to use phototransistors in new applications.

Thank you very much again for support of this effort.

Sincerely yours,

A handwritten signature in cursive script, reading "Harold Fetterman".

Harold Fetterman

Microwave – Optical Interactions

ASSERT – 95

F49620 – 95 –1 – 0429

The ASSERT Program on Microwave – Optical interactions covered a wide range of actual device development. In particular we focused to a great degree on new types of detectors and high frequency optical mixers.

Included in this report are two approaches to traveling wave phototransistors that were developed with the idea that one could achieve both high power and high speed in a novel traveling wave structure. The use of polymer waveguide to bring light into the base of a heterojunction transistor was the key element.

The phototransistors worked relatively well and could operate at high powers at frequencies as high as 60 GHz. There were, and still remain, significant questions in terms of noise and sensitivity.

In a related effort we also looked at optical mixing in high frequency ELO HEMT devices up to 140 GHz. This was an interesting effort and indicates that various materials can be combined for integrated structures. Other efforts using pseudomorphic InP HEMTs with 50 nm gates were successful up to 211 GHz and set a record at the time.

Finally, we also extended our high frequency modulators in this effort. The devices were made to couple to waveguides and modulation was measure up to 110 GHz. Optical mixing techniques, developed earlier in the program, made it possible to make these measurement with a high level of internal calibration. The devices themselves were made in an array, on mylar, and have opened up several new device concepts.

The ASSERT program really helped start this effort on fabricated devices for use in optical – millimeter interactions and its accomplishments are still making contributions to our current high frequency efforts. A selection of papers outlining this work is attached.

Integration of Polyimide Waveguides with Traveling-Wave Phototransistors

D. P. Prakash, D. C. Scott, *Student Member, IEEE*, H. R. Fetterman, *Fellow, IEEE*,
M. Matloubian, *Member, IEEE*, Q. Du, and W. Wang

Abstract—Polymer waveguides with low optical losses are becoming increasingly important for photonic circuits. Among these, polyimide waveguides have properties which distinguish them as a versatile interconnect medium for practical optoelectronic integrated circuits. We have integrated these waveguides with traveling-wave phototransistors (TW-HPT's) in which optical power transfer occurs through leaky mode coupling of light from the waveguide along the length of the device. Independent optimization of the waveguide and phototransistor is now possible permitting superior coupling efficiency and detector bandwidth. We present proof-of-concept results for a 2-mm-long TW-HPT integrated with a $8 \times 10\text{-}\mu\text{m}$ polyimide waveguide.

Index Terms—Heterojunction bipolar transistors, optical interconnections, phototransistors, polyimide films, traveling-wave devices, waveguides.

I. INTRODUCTION

POLYMER waveguides are being developed for use as optical interconnects in photonic circuits [1]. Polyimide waveguides in particular, because of their versatile characteristics, are finding widespread use in wafer scale applications [2]. In our previous work, we have used on-wafer polyimide waveguides and have demonstrated their bandwidth up to 50 GHz [3]. Discrete optoelectronic circuits were used in these experiments with butt coupling from waveguide to the optical detector. In such hybrid optoelectronic configurations, there is an inherent tradeoff between optical coupling efficiency and the detector bandwidth [4]. Furthermore, detectors illuminated vertically also tend to saturate at low optical powers. The central concern of our current work is to explore, using integrated polyimide waveguides, a horizontal coupling scheme to overcome these problems. Polyimide waveguides have been defined directly on the base and collector mesas of a traveling-wave optical device—the traveling-wave heterojunction phototransistor (TW-HPT). The optical power in these devices is coupled through leaky modes along the length of the device. We have demonstrated the viability of the leaky mode coupling concept experimentally and present preliminary results from

prototype devices including the frequency response up to 20 GHz.

II. COMPARISON OF INTERCONNECT TECHNOLOGIES

Several interconnect technologies are currently available including all-glass [5], silicon-on-insulator [7], and InGaAsP on InP [7]. While these technologies have their merits and find specific applications, they have yet to satisfy the basic requirements needed for wafer scale integration. An ideal on-wafer interconnect: 1) has low input coupling loss when butt coupled from a fiber; 2) has low propagation losses when routing light; 3) incorporates passive single/multimode waveguiding elements for functionality; 4) integrates well with electrooptic modulators; and 5) couples efficiently into photodetectors. Polyimide waveguides have the capacity to satisfy these requirements of ideal interconnects and are also both rugged and durable.

Glass waveguides have the best input coupling losses of 0.1 dB per connection and low absorption losses of 0.05 dB/cm [5]. Although this technology is excellent for passive optical circuits, it is not suitable for integration with active devices. Rib waveguides made with silicon on insulator (SOI) are attractive because of established silicon processing techniques. However, single mode propagation is generally not easily obtainable and losses tend to be high [6]. Optical detectors at 1.3–1.55 μm are not available in silicon and therefore restrict the scope of this technology. InGaAsP quaternary waveguides can be integrated with active devices such as p-i-ns and phototransistors [7], but crystal growth techniques place a limitation on the maximum thickness of the waveguide to 0.5–0.7 μm . This again results in poor mode matching from a fiber input and therefore substantial insertion losses. Also, high-speed electrooptic modulators have yet to be demonstrated in the material systems described above. Polyimides, a class of polymers, are an outstanding alternative. Excellent input coupling between fiber and waveguide can be achieved [8]. Polyimides have very low material losses of 0.09 dB/cm [9], which is among the best reported in the literature. Passive polyimide waveguide structures such as delay elements, power splitters/combiners and repetition rate multipliers have been extensively examined [3]. Recently, polymer modulators with bandwidths in excess of 100 GHz have been demonstrated [10]. Through serial grafting techniques [11], polyimide waveguides are ideally suited for integration with such high bandwidth polymer modulators.

Manuscript received February 14, 1997. This work was supported by the Air Force Office of Scientific Research (AFOSR) and by the National Center for Integrated Photonics Technology (NCIPT).

D. P. Prakash, D. C. Scott, and H. R. Fetterman are with the Electrical Engineering Department, University of California, Los Angeles, CA 90024 USA.

M. Matloubian is with Hughes Research Laboratories, Malibu, CA 90265 USA.

Q. Du and W. Wang are with Columbia University, New York, NY 10027 USA.

Publisher Item Identifier S 1041-1135(97)04067-6.

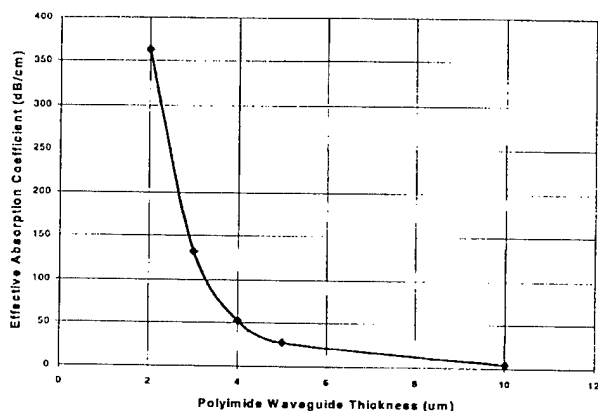


Fig. 1. Simulations of effective absorption coefficient versus polyimide waveguide thickness on InGaAs at 1.3 μm .

III. INTEGRATION WITH TRAVELING-WAVE HETEROJUNCTION BIPOLAR TRANSISTORS

To investigate the potential of polyimide waveguides for efficient optical coupling to active devices, we propose to utilize the traveling-wave concepts that have been implemented so successfully in optical modulator technology [10] and extend these concepts to optical detectors. In our approach, we define a leaky-mode polyimide waveguide on top of the active region of the optical detector. Intensity modulated light is coupled into the polyimide waveguide and leaks into the detector's active region along the length of the device due to the fact that the index of refraction of the semiconductor is higher than that of the polyimide. A microwave signal is generated on the transmission line as light is absorbed by the detector. The bandwidth limitation of such a device is based on the velocity mismatch between the optical wave and the induced electrical microwave [12].

In our traveling-wave approach, the optical absorption can be optimized without degrading the bandwidth. The rate at which the light couples to the device and is absorbed can be described by an effective absorption coefficient and can be adjusted by varying the dimensions of the polyimide waveguide. Therefore, we expect superior coupling efficiency and bandwidth from a waveguide-fed TW-HPT.

To investigate this concept, we used a simulation program by Rsoft, Inc., called BeamProp which is based on the beam propagation method. We simulated structures consisting of polyimide waveguides of various thicknesses on top of $\text{In}_{0.53}\text{Ga}_{0.47}\text{As}$ to extract the effective absorption coefficient at an optical wavelength of 1.3 μm . The index of refraction of the polyimide and InGaAs was 1.52 and 3.368, respectively. The results are shown in Fig. 1 and demonstrate the large range of control over the effective absorption coefficient which leads to design flexibility for varying the length of the detector to achieve optimal optical absorption.

To verify our concept of leaky mode coupling, we coupled light of 1.06- μm wavelength into a 7- μm -thick by 5- μm -wide polyimide waveguide patterned on $\text{In}_{0.53}\text{Ga}_{0.47}\text{As}$. The effective absorption coefficient was determined by measuring the loss/cm using a CCD camera. The results are

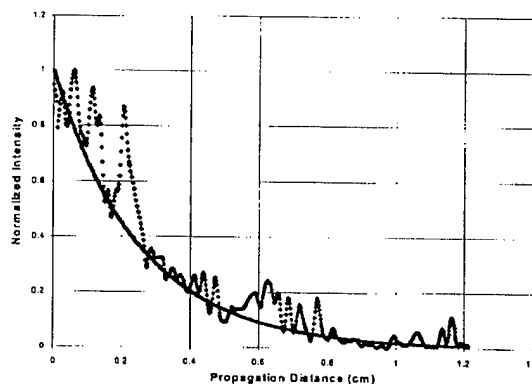


Fig. 2. Experimental verification of leaky-mode coupling using 7- μm -thick polyimide waveguide on InGaAs. Points represent actual measurement data. Solid line is an exponential fit to the data. Effective absorption coefficient measured to be 17 dB/cm.

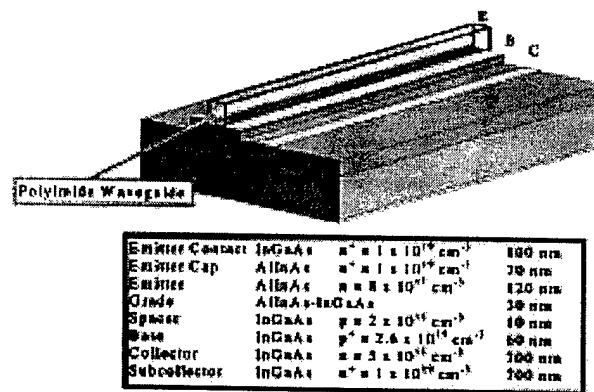


Fig. 3. Device layer structure and diagram of TW-HPT showing polyimide waveguide defined on top of the base mesa.

shown in Fig. 2 and yield an effective absorption coefficient of 17 dB/cm, which agrees well with our simulations.

IV. FABRICATION OF WAVEGUIDE-FED TW-HPT

The fabricated prototype device is shown in Fig. 3. The phototransistor was fabricated first based on an HBT layer structure and then the waveguides were patterned. The device consists of 2-mm-long coupled microstrip lines with electrode widths of 20 μm and separation between lines of 15.11 μm designed for 50- Ω characteristic impedance. On both ends of the device area, the electrodes flare out to dimensions that are compatible with 100- μm -pitch coplanar probes.

In defining polyimide waveguides, we have found it convenient to use Amoco's Ultradel 9120D photoimageable polyimide. Waveguides with smooth and vertical sidewalls were easily achieved using standard photolithography. The polyimide curing was done at a low temperature of 175 $^{\circ}\text{C}$ for 120 min to reduce the possibility of beryllium diffusion from the base to the emitter. The devices were cleaved at liquid nitrogen temperatures to achieve good optical end faces on the polyimide waveguides.

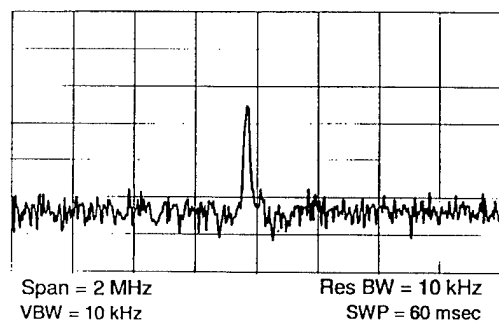


Fig. 4. Spectrum analyzer trace of the 20-GHz optically generated signal with 25-dB SNR. Incident total laser power was 2 mW.

V. EXPERIMENTAL RESULTS AND DISCUSSION

To measure the dc-optical gain of the TW-HPT, light at $1.3\text{-}\mu\text{m}$ wavelength from a single-mode optical fiber was butt coupled to the polyimide waveguides. The response of the TW-HPT varied depending on which optical waveguide was used. When injecting into the bottom waveguide, which is defined on the subcollector, no optical gain was observed. The authors attribute this to the fact that the absorption of light in the subcollector does not effectively change the base-emitter junction potential [13]. However, when light was injected into the top waveguide, which was defined on top of the base, we measure an optical gain of 4.5. The fact that this number is greater than 1 shows the appreciable advantage that HBT based detectors can have over conventional p-i-n detectors. The optical gain can be improved in future generation devices by mode matching the optical waveguide to the input optical fiber and by optimizing the effective absorption coefficient to the device length to obtain $>90\%$ absorption. Presently, we estimate our input coupling loss to be -4.2 dB and our absorption efficiency to be 50% .

Preliminary measurements of the TW-HPT show good frequency response up to 20 GHz with a signal-to-noise ratio (SNR) of 25 dB as indicated in Fig. 4. The frequency response of the device was measured using optical heterodyning of two-tunable diode pumped YAG lasers at $1.3\text{ }\mu\text{m}$ [13]. The bandwidth is currently limited by velocity mismatch, microwave propagation loss, and poor impedance matching to the external circuit. Based on our simulations, the effective index of the microwave transmission line is $n_{\text{mic}} = 2.6$ and the effective index of the optical wave is $n_{\text{opt}} = 1.68$. Ignoring the effects of dispersion, this velocity mismatch limits the theoretical maximum frequency response of our device to 4 GHz-cm. In our case, the optical wave travels faster than the electrical wave. One method for reducing the velocity of the optical beam is by defining gratings in the polymer waveguide which can effectively slow down the k -vector of the optical wave. Optical gratings in polymer waveguides have been successfully demonstrated by B. L. Volodin *et al.* [14]. The full theoretical model and computer simulations of the performance of the TW-HPT will be presented in a subsequent publication.

VI. CONCLUSION

We envision widespread applications of polymer waveguide technology in future photonic and optoelectronic integrated circuits. To integrate polyimide waveguides with detectors, we have explored the concept of leaky mode coupling along the length of a suitable traveling-wave device—the TW-HPT. A prototype device was fabricated with polyimide waveguides defined on the base and collector mesas of a TW-HPT. The leaky mode coupling concept was experimentally verified and shown to be viable. Preliminary results of the waveguide-fed TW-HPT, including a frequency response up to 20 GHz, are presented and discussed. Future work includes the use of slow wave structures in the polyimide waveguide for velocity matching and the design of broad-band, low-loss, matched microwave transmission lines.

ACKNOWLEDGMENT

The authors thank K. Medlock and K. Medlock of Pixel for loan of an Apogee AM4 camera used in our measurements.

REFERENCES

- [1] B. L. Booth, "Low loss channel waveguides in polymers," *J. Lightwave Technol.*, vol. 7, pp. 1445–1453, Oct. 1989.
- [2] H. R. Fetterman, D. P. Prakash, D. C. Scott, and W. Wang, "Integrated optically driven microwave/millimeter wave device structures," in *IEEE MTT-S Int. Microwave Symp. Dig.*, May 1994, vol. 3, pp. 1493–1496.
- [3] D. P. Prakash, D. V. Plant, D. Zhang, and H. R. Fetterman, "Optical transmission of millimeter wave signals through polyimide channel waveguides fabricated using direct laser writing," in *SPIE, Nonconducting Photopolymers and Appl.*, July 1992, vol. 1774, pp. 118–129.
- [4] R. J. Deri, "Monolithic integration of optical waveguide circuitry with III-V photodetectors for advanced lightwave receivers," *J. Lightwave Technol.*, vol. 11, pp. 1293–1313, Aug. 1993.
- [5] Product Literature, Photonic Integration Research Inc., Columbus, OH, 1996.
- [6] A. G. Rickman, G. T. Reed, and F. Namavar, "Silicon-on-insulator optical rib waveguide loss and mode characteristics," *J. Lightwave Technol.*, vol. 12, pp. 1771–1776, Oct. 1994.
- [7] P. Freeman, X. Zhang, I. Vurgaftman, J. Singh, and P. Bhattacharya, "Optical control of 14 GHz MMIC oscillators based on InAlAs/InGaAs HBT's with monolithically integrated optical waveguides," *IEEE Trans. Electron Devices*, vol. 43, pp. 373–379, Mar. 1996.
- [8] A. Chen, V. Chuyanov, F. I. Marti-Carrera, S. Garner, W. H. Steir, J. Chen, S. Sun, and L. R. Dalton, "Integrated polymer waveguide mode size transformer with a vertical taper for improved fiber coupling," in *SPIE Proc.*, to be published.
- [9] Ultradel 9120D Bulletin, Amoco Chemical Company, Naperville, IL.
- [10] D. Chen, H. R. Fetterman, A. Chen, W. H. Steir, L. R. Dalton, W. Wang, and Y. Shi, "High-bandwidth polymer modulators," in *SPIE*, vol. 3006, pp. 314–317, Feb. 1997.
- [11] T. Watanabe, M. Amano, M. Hikita, Y. Shuto, and S. Tomaru, "Novel 'serially grafted' connection between functional and passive polymer waveguides," *Appl. Phys. Lett.*, pp. 1205–1207, Sept. 1994.
- [12] V. M. Hietala, G. A. Vawter, T. M. Brennan, and B. E. Hammons, "Traveling-wave photodetectors for high-power, large-bandwidth applications," *IEEE Trans. Microwave Theory Tech.*, vol. 43, pp. 2291–2297, Sept. 1993.
- [13] D. C. Scott and H. R. Fetterman, "Millimeter wave generation using InP HBT phototransistors," in *InP HBTs: Growth, Processing, and Applications*, B. Jalali and S. J. Pearton, Eds. Boston, MA: Artech House, 1995, ch. 10.
- [14] B. L. Volodin, B. Kippelen, K. Meerholz, N. V. Kukhtarev, H. J. Caulfield, and N. Peyghambarian, "Non-Bragg orders in dynamic self-diffraction on thick phase gratings in a photorefractive polymer," *Opt. Lett.*, vol. 21, no. 7, pp. 519–521, 1996.

High-Power High-Frequency Traveling-Wave Heterojunction Phototransistors with Integrated Polyimide Waveguide

D. C. Scott, D. P. Prakash, H. Erlig, D. Bhattacharya, M. E. Ali,
H. R. Fetterman, *Fellow, IEEE*, and M. Matloubian, *Member, IEEE*

Abstract—A high-power high-speed phototransistor has been demonstrated using a traveling-wave (TW) structure with an integrated polyimide optical waveguide. In our configuration, optical power transfer is distributed along the length of the device via leaky mode coupling of light from the polyimide waveguide to the active region of the phototransistor. The TW electrode design allows for an electrically long structure while maintaining high bandwidths. Due to the increased absorption volume, the optical power handling capabilities of the TW-heterojunction phototransistors (TW-HPT's) are improved over that of conventional lumped-element HPT detectors. The experimental results show no saturation of the fundamental at 60 GHz up to 50 mA of dc photocurrent.

I. INTRODUCTION

ONE of the major commercial incentives driving research in photonics is the microwave fiber optic link. A typical link consists of a laser source, an external modulator, the fiber optic transmission medium, and an optical detector. High-frequency optical detectors are one of the primary components that dictate the system performance of the fiber optic link. In order to reduce the radio frequency (RF) insertion loss, increase the spurious free dynamic range, and increase the signal-to-noise ratio of the link, the photodetector needs to be able to handle high optical powers [1]. Heterojunction phototransistors (HPT's) which exhibit optical gain via transistor action offer improvements in link gain over p-i-n or MSM photodiodes. Although much work has been done on high-speed phototransistors [2], a classic design conflict exists between the simultaneous optimization of high-frequency performance and optical coupling efficiency. In lumped-element HPT's, the devices need to be scaled down in size for high-speed operation. These small devices tend to saturate at low input optical power levels because of the small absorption volume.

Manuscript received April 1, 1998. This work was supported by the Air Force Office of Scientific Research (AFOSR) and by the National Center for Integrated Photonics Technology (NCIPT).

D. C. Scott was with the Electrical Engineering Department, University of California, Los Angeles, CA 90095-1594 USA. He is now with TRW, Redondo Beach, CA 90278 USA.

D. P. Prakash was with the Electrical Engineering Department, University of California, Los Angeles, CA 90095-1594 USA. He is now with IBM, Essex Junction, VT 05452-4299 USA.

H. Erlig, D. Bhattacharya, M. E. Ali, and H. R. Fetterman are with the Electrical Engineering Department, University of California, Los Angeles, CA 90095-1594 USA.

M. Matloubian is with HRL, Malibu, CA 90265 USA.

Publisher Item Identifier S 1051-8207(98)05621-9.

In an attempt to overcome these problems, we propose to utilize the traveling-wave (TW) concepts that have been implemented so successfully in optical modulator technology and extend these concepts to HPT detectors. A schematic diagram of our TW heterojunction phototransistor (TW-HPT) is shown in Fig. 1. In our approach, we define a leaky-mode polyimide waveguide on top of the active region of the HPT. Intensity-modulated light is coupled to the polyimide waveguide and leaks into the HPT's active region along the length of the device due to the fact that the index of refraction of the semiconductor is higher than that of the polyimide. The metal pads of the HPT are coplanar waveguide with the center line contacting the emitter and the ground plane contacting the collector. The base is floating. A microwave signal is generated on the transmission line as light is absorbed along the length of the detector. The ultimate bandwidth limitation of such a device is based on the velocity mismatch between the optical wave and the induced electrical microwave [3]–[6].

Due to the integration of the polyimide waveguide and the HPT in the TW configuration, power saturation effects are improved because the absorption of the incident light signal is distributed along the entire length of the device. The layer structure for the TW-HPT is a typical HBT design consisting of a 600-Å base with a graded base-emitter junction [7]. The polyimide optical waveguide is defined on top of the emitter and lies in the gap between the center electrode and the ground plane. Since the core size for single mode fiber at an optical wavelength of 1.3 μm is approximately 9 μm , we chose the dimensions of the polyimide waveguide to be 10 \times 10 μm . A second set of devices was also fabricated in which the center electrode shorted the emitter to the base to form a diode structure. We will refer to this device as TW-Diode. The optical absorption interaction length between the waveguide and the HPT device was varied from 20, 200, to 2000 μm .

II. EXPERIMENTAL RESULTS

The dc optical responses of the TW-HPT and TW-Diode are shown in Fig. 2(a) and (b), respectively. A bias voltage of $V_{ce} = 1.5$ V was applied to all devices. Comparing the two figures, it is evident that the transistor action of the TW-HPT dramatically increases the sensitivity of the optical response. The optical gain G is as high as 13.5 for the 2-mm-long TW-HPT as opposed to $G = 0.374$ for the diode. For a given

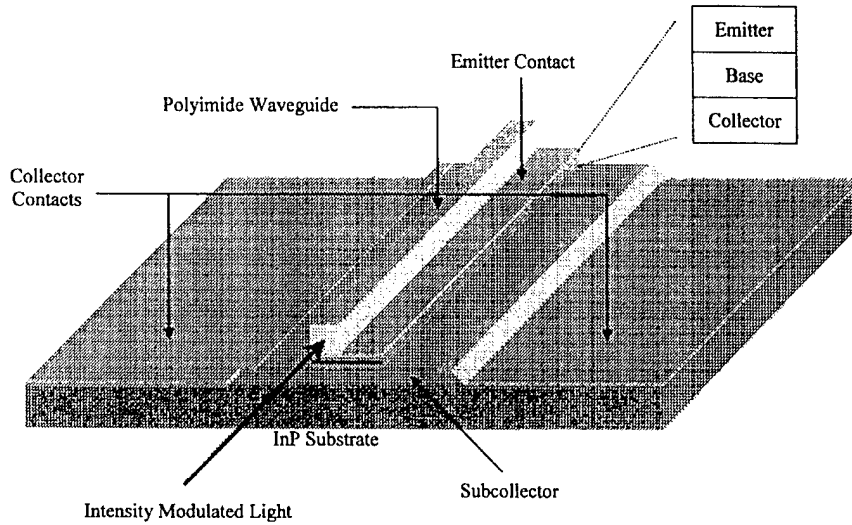
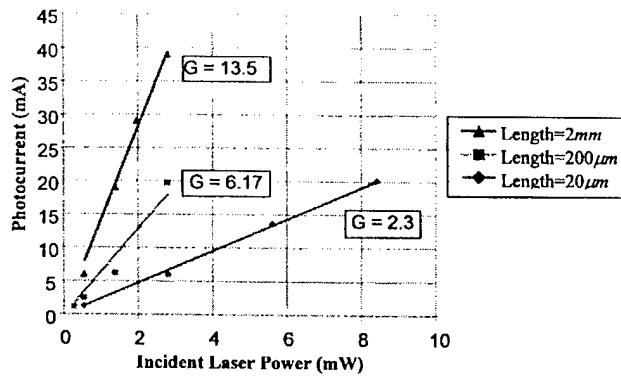
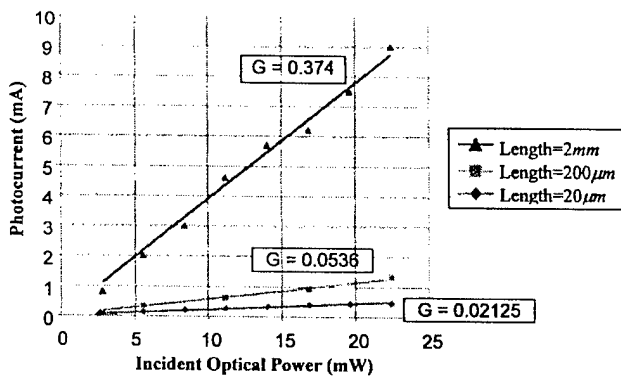


Fig. 1. Schematic diagram of the TW-HPT. Polyimide waveguide is defined on top of the active region of an HPT. The HPT's electrodes are coplanar waveguide with a characteristic impedance of 50 Ω .



(a)



(b)

Fig. 2. DC optical response of the (a) TW-HPT and (b) TW-Diode.

optical power of 2.8 mW, the 2-mm-long diode photocurrent is 0.8 mA, but the corresponding transistor photocurrent is 40 mA, which is 50 times larger. In all cases the induced photocurrent increases linearly with increasing optical power indicating that the devices are not saturating.

By measuring the photocurrent as a function of device length for a given optical power, we can estimate the input

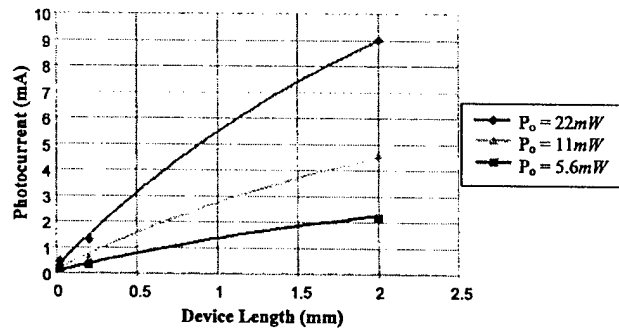


Fig. 3. Photocurrent as a function of TW-Diode device length for three different incident optical powers. The solid lines are the theoretical fit to the data.

optical coupling efficiency. This is most easily accomplished with the diode since the transistor gain can vary from device to device. The results for the TW-Diode are shown in Fig. 3 for three different input optical powers. The solid lines are a theoretical fit to the measured data based on the equation

$$I_{ph} = \frac{q\eta}{h\nu} P_o. \quad (1)$$

I_{ph} is the optically generated portion of the output current, P_o is the incident optical power, q is the electronic charge, $h\nu$ is the energy of the incident photons, and η is the external quantum efficiency. The external quantum efficiency can be broken up into separate factors that describe the different mechanisms for light loss and light absorption:

$$\eta = \eta_{\text{coupling}} \cdot \eta_{\text{propagation}} \cdot \eta_{\text{leaky}} \quad (2)$$

where η_{coupling} is the input coupling loss between the optical fiber and the polyimide waveguide, $\eta_{\text{propagation}}$ is the propagation loss from the optical input of the device to the active region, and η_{leaky} is the amount of light absorption that occurs in the active region via the leaky mode coupling mechanism. $\eta_{\text{propagation}}$ is difficult to estimate so we will

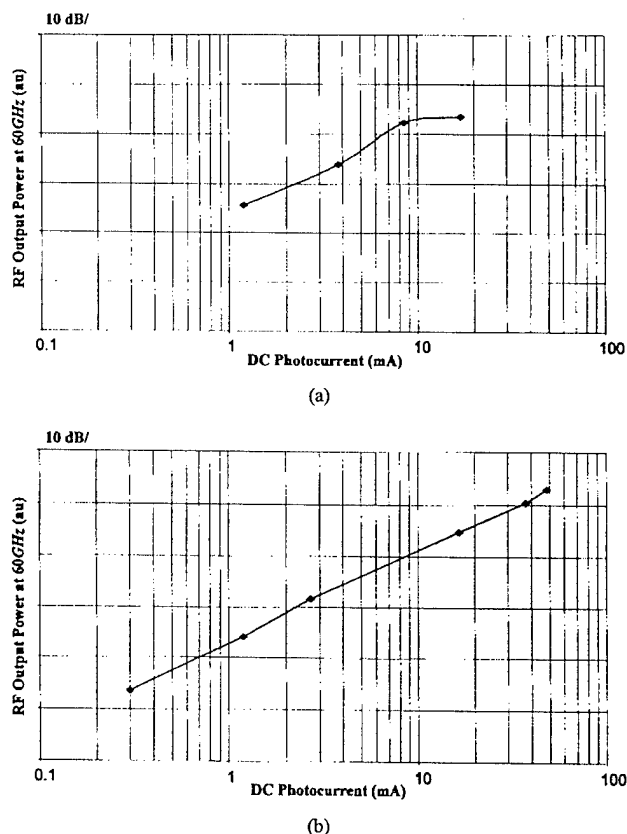


Fig. 4. Optical power saturation at 60 GHz for (a) lumped-element HPT and (b) 200- μm -long TW-HPT.

combine $\eta_{\text{propagation}}$ with η_{coupling} and define this as the total input coupling loss prior to the active region of the device. η_{leaky} can be written mathematically as

$$\eta_{\text{leaky}} = 1 - e^{-\alpha_{op}l} \quad (3)$$

where α_{op} is the effective absorption coefficient which is determined by the thickness of the polyimide waveguide and l is the length of the active region. Plugging in (2) and (3) into (1) we obtain

$$(I_{ph} = \frac{qP_o}{h\nu} \eta_{\text{coupling}} (1 - e^{-\alpha_{op}l}). \quad (4)$$

Given that our polyimide waveguide thickness was measured to be 7.5 μm , the effective optical absorption coefficient given by our previously published simulations is taken to be $\alpha_{op} = 4 \text{ cm}^{-1}$ [7]. We can now fit (4) to the measured data of the 20- μm -, 200- μm -, and 2-mm-long TW-Diodes as shown in Fig. 3 and determine our input coupling efficiency to be $\eta_{\text{coupling}} = 70\%$.

The optical power saturation measurements for the TW-HPT's were made at 60 GHz using two diode-pumped Nd:YAG lasers in an optical mixing configuration at a wavelength of 1.3 μm . The results are presented for the 200- μm -long device since this seemed to exhibit the best trade-off between device length and performance. The results for the TW-HPT were compared to a lumped-element HPT that was fabricated with a similar layer structure and had an emitter area of $8 \times 8 \mu\text{m}$. The displayed data in Fig. 4 shows that the lumped-element HPT output signal begins to saturate at a dc photocurrent of 8 mA whereas the 200- μm -long TW-HPT shows no signs of saturation up to 50 mA. The power-handling ability of the TW-HPT is superior to that of the lumped-element HPT due to the distributed nature of the optical absorption via the leaky mode configuration.

III. CONCLUSION

We experimentally measured the optical response of the TW-HPT and demonstrated high optical gains with input optical coupling efficiencies of 70%. A 200- μm -long TW-HPT exhibited no output power saturation up to 50 mA of dc photocurrent at an operating frequency of 60 GHz. We envision widespread applications of the high-power high-frequency TW-HPT in future photonic and optoelectronic integrated circuits.

REFERENCES

- [1] L. Lembo, F. Alvarez, D. Lo, C. Tu, P. Wiseman, C. Zmudzinski, and J. Brock, "Optical electroabsorption modulators for wideband, linear, low-insertion loss photonic links," in *Proc. SPIE*, vol. 2481, 1996, pp. 185-196.
- [2] S. Chandrasekhar, M. K. Hoppe, A. G. Dentai, C. H. Joyner, and G. J. Qua, "Demonstration of enhanced performance of an InP/InGaAs heterojunction phototransistor with a base terminal," *IEEE Electron Device Lett.*, vol. 12, Oct. 1991.
- [3] L. Y. Lin, M. C. Wu, T. Itoh, T. A. Vang, R. E. Muller, D. L. Sivco, and A. Y. Cho, "High-power high-speed photodetectors—Design, analysis, and experimental demonstration," *IEEE Trans. Microwave Theory Tech.*, vol. 45, pp. 1320-1331, Aug. 1997.
- [4] H. F. Taylor, O. Eknoyan, C. S. Park, K. N. Choi, and K. Chang, "Traveling wave photodetectors," in *Proc. SPIE, Optoelectronic Signal Processing for Phased-Array Antennas II*, 1990, vol. 1217, pp. 59-63.
- [5] V. M. Hietala, A. Vawter, T. M. Brennan, and B. E. Hammons, "Traveling-wave photodetectors for high-power, large-bandwidth applications," *IEEE Trans. Microwave Theory Tech.*, vol. 43, pp. 2291-2297, Sept. 1995.
- [6] K. S. Giboney, R. L. Nagarajan, T. E. Reynolds, S. T. Allen, R. P. Mirin, M. J. W. Rodwell, and J. E. Bowers, "Travelling-wave photodetectors with 172-GHz bandwidth and 76-GHz bandwidth-efficiency product," *IEEE Photon. Technol. Lett.*, vol. 7, pp. 412-414, Apr. 1995.
- [7] D. P. Prakash, D. C. Scott, and H. R. Fetterman, "Integration of polyimide waveguides with traveling wave phototransistors," *IEEE Photon. Technol. Lett.*, vol. 9, pp. 800-802, June 1997.

The Optical Response of Epitaxial Lift-Off HEMT's to 140 GHz

Daipayan Bhattacharya, Hernan Erlig, Mohammed E. Ali, Shamino Wang, Harold R. Fetterman, *Fellow, IEEE*, Richard Lai, and Dwight C. Streit, *Senior Member, IEEE*

Abstract—We present measurements on the optical frequency response of epitaxial lift-off (ELO) 1.0- μm InP high-electron mobility transistors (HEMT's) to 140 GHz using electrooptic sampling and heterodyne techniques. Our picosecond sampling measurements established that the lift-off devices exhibited substantial optical response to 140 GHz. Heterodyne measurements made at 60 and 94 GHz later confirmed these findings. A novel three wave mixing technique was used to extend the heterodyne bandwidth to 130 GHz. In these experiments, millimeter waves were generated in our optically driven HEMT's and launched into waveguides. These lift-off devices can be major additions to future millimeter wave integrated optoelectronic systems either as high frequency optical detectors or as optically driven tunable millimeter wave sources.

Index Terms— Electrooptic measurements, epitaxial lift-off, integrated optoelectronics, millimeter wave generation, MODFET's, optical mixing, picosecond sampling.

I. INTRODUCTION

OF ALL THE techniques that have been studied to integrate electrical and optical circuits, including flip-chip bonding, wafer bonding, and heteroepitaxy, epitaxial lift-off (ELO) has shown itself to be particularly versatile. Devices from different material systems can be combined by releasing the epitaxially grown layers from their original substrate and grafting them to virtually any other suitable substrate. In the past, researchers have shown the effectiveness of this technique with numerous material systems, including semiconductor to semiconductor [1], semiconductor to glass [2], semiconductor to sapphire, and semiconductor to diamond [3], among others.

One class of devices which are important elements in all optoelectronic systems, namely semiconductor photodetectors, stand to benefit greatly from ELO technology. Prior research has shown that little degradation occurs in the optical [4] or electrical response [5] of devices after lift-off at microwave frequencies. Recently, largely because of WDM communication applications, there has been a push to develop optical systems that can work at millimeter wave frequencies. The ef-

fect of the grafting process on the millimeter wave response of high-frequency photodetectors, investigated here, is therefore a critical area of research for future integrated devices.

A continuous challenge to researchers in the field of ultrafast optoelectronic devices has been the ability to accurately measure their response. Two techniques that have been widely used are optical heterodyne and picosecond electrooptic sampling. Picosecond electrooptic sampling offers excellent linearity, the ability to characterize a calibrated high-frequency response, and minimal intrusion on the circuit which is being measured. Optical heterodyne, on the other hand, has the advantages of being highly sensitive and has the capability of examining important device applications.

In this paper, we measure the optical response of 1- μm InP ELO PHEMT's on quartz substrates to 140 GHz using both picosecond electrooptic sampling and optical heterodyne characterizations. In our picosecond measurements, a novel technique is used, whereby we sample directly from commercial coplanar probes. This makes it unnecessary to wire bond or connect coplanar lines to the device for minimally invasive probing. Our sampling results establish that the lift-off process does not adversely affect the high-frequency optical response of the high-electron mobility transistor (HEMT) photodetectors to 140 GHz. Optical heterodyne experiments at 60, 94, and 130 GHz provide further confirmation of this. The extension of our heterodyne experiments to 130 GHz utilizes a three-wave mixing technique. To our knowledge, this is the highest frequency optical mixing to date and confirms the use of lift-off HEMT's as high-frequency optical detectors. These devices can be readily integrated into millimeter wave optoelectronic systems by using ELO configurations.

II. DEVICE PARAMETERS AND FABRICATION

A cross section of the layer structure of our 1- μm gate HEMT's is shown in Fig. 1. The layers of the device were grown on an InP substrate using molecular beam epitaxy (MBE). The 20-nm InGaAs capping layer was heavily doped to allow for good low-resistance ohmic contacts to the source and drain and to protect the donor layer from surface oxidation. The 20-nm InAlAs donor layer was planar doped with Si at a level of $3.66 \times 10^{12} \text{ cm}^{-3}$. A small 2-nm undoped InAlAs layer was included to further separate the 2DEG channel electrons from coulombic interactions with the ionized dopant atoms in the donor layer. A 15-nm undoped $\text{In}_{0.7}\text{Ga}_{0.3}\text{As}$ pseudomorphic layer was used as the 2DEG channel. Hall mobility measurements on the samples yielded channel mobilities of

Manuscript received October 7, 1996; revised May 5, 1997. This work was supported by the Air Force Office of Scientific Research under the direction of H. R. Schlossberg, by the University of California and TRW MICRO, and by the National Center for Integrated Photonics Technology.

D. Bhattacharya, H. Erlig, M. E. Ali, S. Wang, and H. R. Fetterman are with the Department of Electrical Engineering, University of California, Los Angeles, CA 90095 USA.

R. Lai and D. C. Streit are with the TRW Electronic Systems and Technology Division, Electronic Systems Group, Redondo Beach, CA 90278 USA.

Publisher Item Identifier S 0018-9197(97)06230-1.

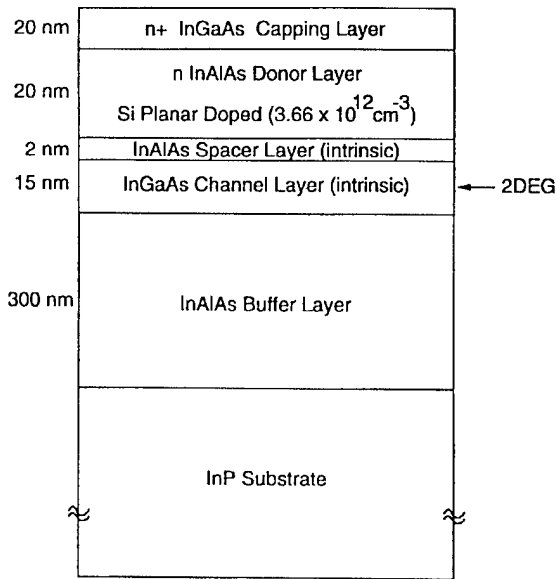


Fig. 1. Cross section of pseudomorphic epitaxial lift-off high-electron mobility transistor, detailing layer structure.

$10860 \text{ cm}^2/\text{V}\cdot\text{s}$ at 300 K. Finally, a 300-nm InAlAs buffer layer was included to serve as an etch stop in the epitaxial lift-off process.

The process of preparing the ELO films involved two distinct steps. The removal of the processed device film from its original substrate and the subsequent attachment of the thin film onto a host substrate. For devices fabricated on the InP material system, the etch selectivity of hydrochloric acid (HCl) for InP versus InAlAs was exploited. In this method, the entire backside of the substrate can be etched away. The InAlAs buffer layer acts as an etch stop, preventing damage to the active device layers. Our device wafers were mechanically thinned and polished to $50 \mu\text{m}$ prior to etching. This allowed for better control of the use of the etch stop by using dilute concentrations of HCl while still maintaining reasonable etch times. The sample was then covered with Apiezon W wax (black wax) which was dissolved in trichloroethylene (TCE). By dissolving the wax in TCE, the proper consistency was achieved to allow the wax to flow to the edges of the sample. The main functions of the black wax were to protect the top layers of the device from the etchant and to give the thin film mechanical stability during the time it was removed from the substrate till it was attached to the host substrate. Immersion of the sample in HCl for about 6 min sufficed to etch away the $50\text{-}\mu\text{m}$ substrate.

For our measurements, we chose quartz as a host substrate since it is transparent and has low microwave loss. For the optical heterodyne experiments, the thin film devices were attached to the quartz using Van der Waals' forces. In this process, the device, supported by the black wax, is allowed to dry under weight for about 24 h. Attractive forces between the substrate and the semiconductor squeeze out the water until short-range Van der Waals' forces hold the two together [6]. Van der Waals bonding is a very versatile technique in that any semiconductor material can be attached to almost any

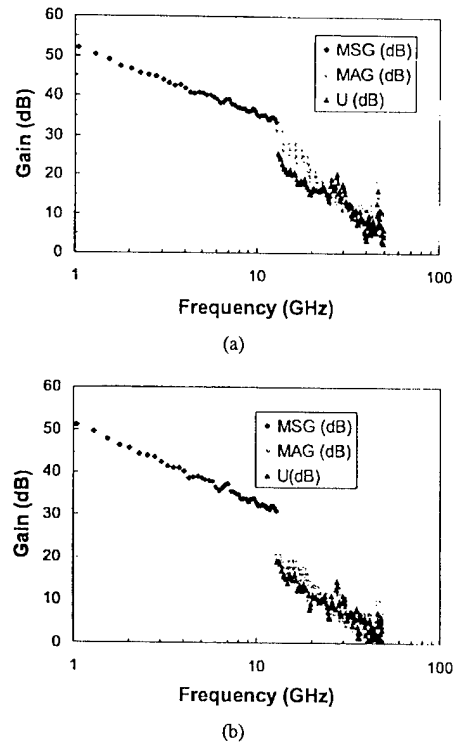


Fig. 2. Electrical gain response [maximum available gain (MAG), maximum stable gain (MSG) and unilateral power gain (U)] of (a) bulk HEMT photodetectors and (b) lift-off HEMT photodetectors were measured on a HP8510C vector network analyzer. By extrapolation of the U data, the f_{max} of the bulk and lift-off devices are found to be 60 and 50 GHz, respectively.

host, given conditions of planarity and cleanliness. However, for our devices, yields of only about 10% were achieved using this Van der Waals bonding approach. Therefore, an alternative attachment method was used for devices used in the electrooptic sampling experiments and the electrical RF measurements. Here an ultraviolet curable optical adhesive was used to attach the film to the substrate. Using this approach, the yield of the grafted film devices improved dramatically. DC electrical measurements showed no difference for the films attached using Van der Waals bonding and optical adhesive bonding.

III. ELECTRICAL CHARACTERIZATION

The electrical response of our devices were characterized by measurements of the peak transconductance and S-parameters on an extended HP8510C vector network analyzer (45 MHz–50 GHz) for both bulk and lift-off devices. The devices were contacted using on-wafer air coplanar probes (Picoprobe Model 67A by GGB Industries Incorporated). For the bulk devices, the maximum extrinsic transconductance g_m was measured to be 29.0 mS at a gate voltage of -0.1 V . For the lift-off devices, the peak g_m was 21.0 mS at a gate voltage of -0.48 V . The S-parameter measurements yielded the gain profiles of the devices, as shown in Fig. 2(a) for the bulk devices and Fig. 2(b) for the lift-off devices. The bulk devices and the lift-off devices had f_{max} 's of 50 and 60 GHz, respectively. Both the bulk and the lift-off devices had f_{TS}

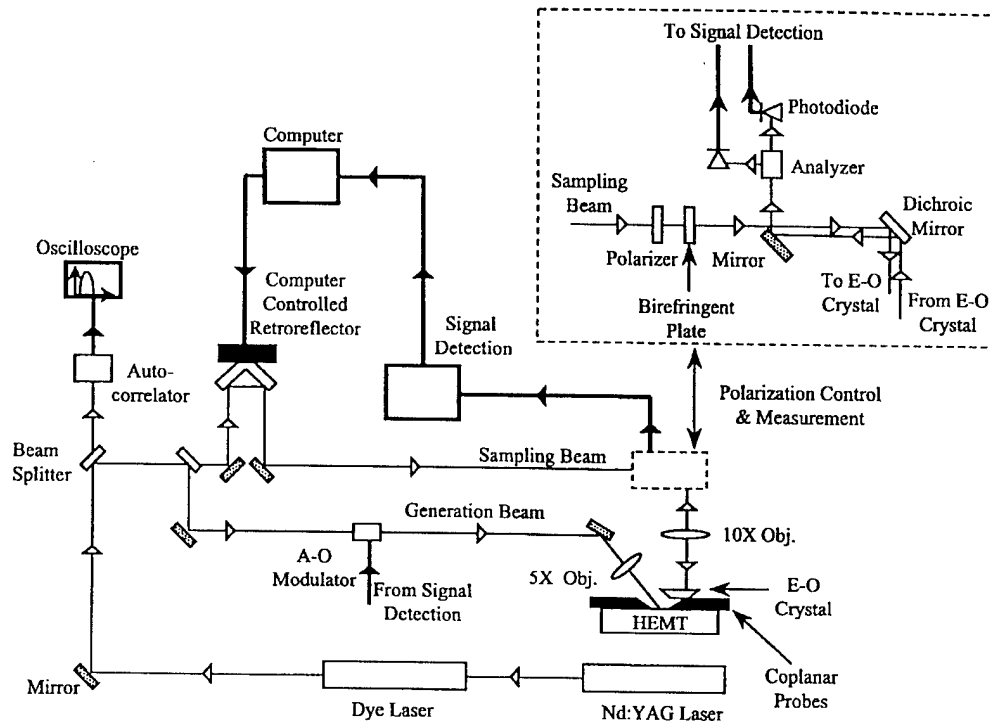


Fig. 3. Electrooptic sampling system schematic. Details of the electrooptic intensity modulator are shown.

of 40 GHz. The electrical response of the lift-off devices are only slightly degraded when compared to the bulk devices.

IV. ELECTROOPTIC SAMPLING TECHNIQUE

A. Experimental Setup and Calibration

To measure the photoresponse of the lift-off HEMT's, an external electrooptic sampling scheme was used, similar to that presented in [7]. A simplified schematic of the pump-probe setup is shown in Fig. 3. The laser system was comprised of a synchronously mode-locked dye laser pumped by the frequency-doubled output of an actively mode-locked Nd:YAG laser. The dye gain medium was Rhodamine 6G and further pulse narrowing was achieved by using a DODCI saturable absorber. The 608-nm output of the dye laser consisted of a pulse train of 1.4-ps full width at half maximum (FWHM) pulses, measured with an autocorrelator, with a repetition rate of 76 MHz and an average power of 115–125 mW. The sampling beam was routed through a corner cube reflector mounted on a computer-controlled translation stage. In this fashion, the timing between the sampling and generation pulses could be controlled. At the input of the electrooptic intensity modulator, the sampling beam average power was maintained at approximately 3.2 mW. After transmission through the acoustooptic modulator, the average generation beam power was 3.4 mW. The intensity of the sampling and generation beams were controlled by attenuators not shown in Fig. 3. At the end of the generation arm, the beam was focused onto the active area of the HEMT using a 5 \times objective lens.

The use of the electrooptic intensity modulator in this sampling application is found in [7] and [8]. A commercial 20- μ m-thick LiTaO₃ crystal (Terametrix Model 200C-TIR) was used to perform the electrooptic modulation. This crystal thickness has been shown to minimize the distortion of the measured signal when compared to thicker crystals [9]. The crystal is in the shape of an inverted truncated pyramid, the faces of which are cut at 60 deg. The angled faces of the crystal make it possible to use total internal reflection to collect the sampling beam for analysis. Both the bulk and lift-off HEMT's were contacted via air coplanar probes (Picoprobe Model 67A). The probes have a 100- μ m pitch and exhibit nearly a 50- Ω impedance from dc to 67 GHz. The photoresponse of the HEMT was sampled by bringing the LiTaO₃ crystal into close proximity of the coplanar probe on the drain side. A schematic representation of this is shown in Fig. 4. The optic axis of the crystal was oriented perpendicular to the center line of the coplanar probe and parallel to the base of the crystal.

Typical half wave voltages, V_{π} , for the intensity modulators used in electrooptic sampling are on the order of kilovolts [10]. Therefore, in order to detect millivolt-level signals, careful attention has to be paid to minimizing noise, which in this case, is largely laser RIN noise. To this end, the mixing approach developed by Chwalek in [11] was used. In this scheme, the relatively small electrooptic intensity modulation is detected differentially. However, if an imbalance exists in the detection system, the amplitude noise of the laser can severely degrade the signal-to-noise ratio (SNR). By modulating the generation beam at high frequencies where the laser amplitude noise is low, the effect of the system imbalance can be minimized (see the Appendix for mathematical derivations). A two-channel RF

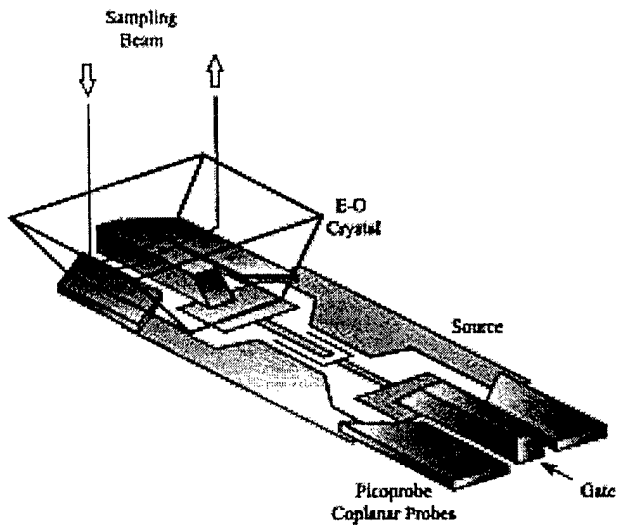
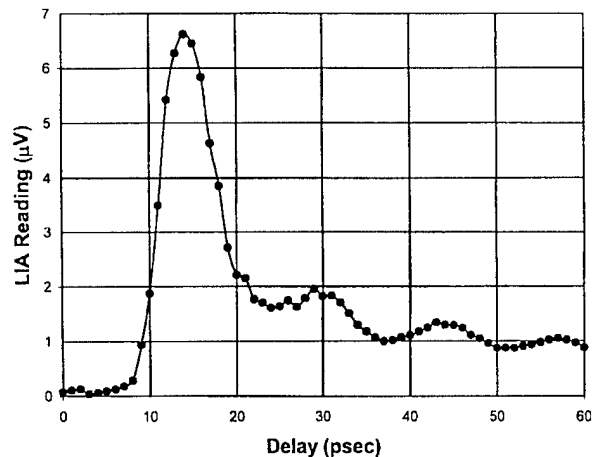


Fig. 4. Schematic of sampling from coplanar probes. The LiTaO₃ crystal is situated over the drain of the device and total internal reflection is used to retrieve the sampling beam.

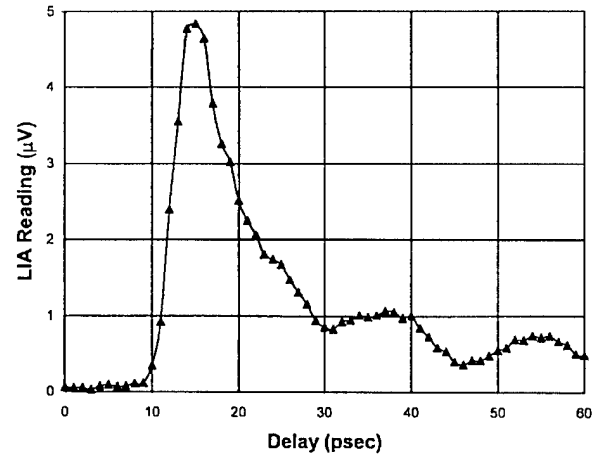
mixer system (Terametrics Model 100-RF) which employed a square wave at 3.000 MHz and a sine wave at 2.998 MHz was used.

To obtain a first-order estimate of the electrooptic signal strength and the SNR, a 6-mm-long coplanar waveguide was contacted at the ends by the coplanar probes and the LiTaO₃ crystal was situated over one of the probes. The 55-Ω coplanar waveguide had a center transmission line width of 50-μm and a center transmission line to ground plane separation of 50-μm. A sinusoidal waveform at 3.000 MHz was applied to one of the coplanar probes and monitored on an oscilloscope. For a sampling beam average power of 3.2 mW and a voltage sinusoid amplitude of 481 mV, the rms voltage detected by the lock-in amplifier (LIA) was 12.75 μV. The equivalent noise voltage was measured to be 223.6 nV/√Hz. For sampling purposes, the lock-in filter bandwidth was chosen to be 1 s and every point was measured 25 times for averaging. These factors considered, the minimum detectable voltage was 1.88 mV.

Because of spatial considerations, the sampling function took place near the end of the crystal. Therefore the electrical transient had to propagate approximately 100 μm through the crystal before reaching the sampling site. Propagation through the crystal causes degradation of the transient being sampled. Furthermore, the high-frequency behavior (beyond 67 GHz) of the coplanar probes was not known. In order to have an estimate of the influence of these effects on the frequency response of the sampling system, a simple comparative test was performed. This involved the fabrication of low-temperature GaAs (LT-GaAs) photoconductive switches imbedded into coplanar waveguide. The coplanar waveguide geometry was identical to that described above. The photoconductive switch gap was 50 μm long and 20 μm wide. The switch was biased at 40 V. The response from the switches was measured under two different sampling conditions. First, the LiTaO₃ crystal was contacted to the coplanar waveguide approximately



(a)



(b)

Fig. 5. Time-domain photoresponse of (a) lift-off HEMT and (b) bulk HEMT. Both responses exhibit a short initial pulse followed by a slowly decaying tail. The pulses have a FWHM of 7.8 and 8.3 ps for the lift-off and bulk HEMT's, respectively. The ripples in the tail are attributed to electromagnetic radiation emitted by the device.

1 mm from the generation site. The sampling site within the crystal was near the entrance face, where the electrical transient entered. The photoresponse in the frequency domain for this sampling condition was $Y_1(\omega)$. Whenever referring to functions or calculations in the frequency domain, it is to be understood that only the amplitude spectra is being used. Second, a coplanar probe was used to contact the coplanar waveguide at approximately 1 mm from the generation site. The LiTaO₃ crystal was situated over the coplanar probe and the sampling site was moved to the end of the crystal. The measured photoresponse in the frequency domain was $Y_2(\omega)$. The electrical transient just before 1 mm from the generation site is assumed to be similar for both sampling conditions. Therefore, any difference in the measured switch response must be due to the two different sampling geometries.

The frequency response comparison estimate can be quantified from the theory of linear systems

$$\frac{Y_2(\omega)}{Y_1(\omega)} = \frac{H_2(\omega)X(\omega)}{H_1(\omega)X(\omega)} = \zeta(\omega) \quad (1)$$

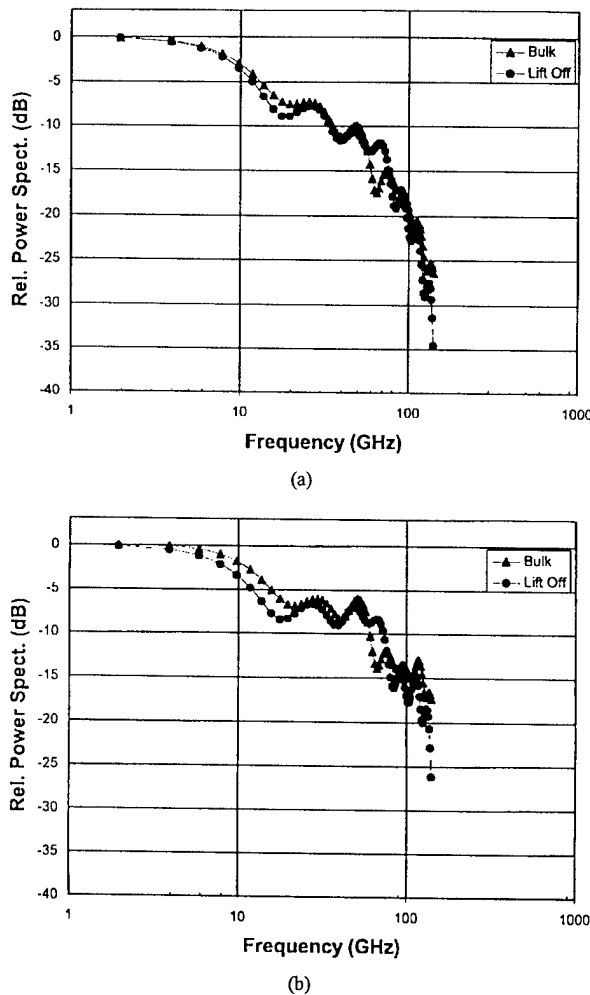


Fig. 6. (a) Lift-off and bulk HEMT relative power spectrum to 140 GHz obtained from time-domain data and (b) calibrated lift-off and bulk HEMT relative power spectrum to 140 GHz using (3) and the calibrating function, $\zeta(\omega)$. Beyond 30 GHz, the calibrated response shows an improvement over the uncalibrated data. At 140 GHz, the improvement is approximately 10 dB. The ripple in the response is attributed to the tails present in the time-domain response.

where $H_1(\omega)$ is the sampling system frequency response for sampling condition one, $H_2(\omega)$ is the system frequency response for sampling condition two, and $X(\omega)$ is the Fourier transform of the electrical transient just before 1 mm from the generation site. The function $\zeta(\omega)$, the system frequency response ratio, was calculated to 140 GHz. Beyond 80 GHz, $\zeta(\omega)$ shows a sharp roll off and at 140 GHz its value is 0.375 of that at dc.

B. HEMT Optical Frequency Response Measurements

For the optical response measurements, the drain to source bias on the lift-off and bulk devices was 2.0 V. Typically, a moderate negative bias must be applied on the gate in order to obtain a fast photoresponse from HEMT's. As the negative bias on the gate increases, such that the transconductance approaches zero, the photoresponse speed increases [12]. Our dc measurements show the transconductance for both the lift-off and bulk devices approaches 0 S at approximately -1.0

V gate to source. Therefore, for the measurements presented here the gate to source bias for both lift-off and bulk HEMT's was set to -4.0 V.

For the specified bias conditions, the photoresponse in the time domain is shown in Fig. 5(a) and 5(b) for the lift-off and bulk HEMT's, respectively. Qualitatively the photoresponse from the lift-off and bulk device are similar. Both exhibit an initial short pulse followed by a slowly decaying tail, these results are in agreement with those found in [13]. The tail is attributed to the collection of slow moving photogenerated holes. The magnitude of the tail and therefore its influence on the photoresponse is a strong function of the gate bias. This trend was experimentally observed in a set of preliminary measurements, where the tail amplitude decreased as the negative bias on the gate increased. For the lift-off HEMT's the photoresponse pulse exhibits a FWHM of 7.8 ps; while for the bulk devices the pulse exhibits a 8.3-ps FWHM.

Due to the probing geometry, part of the LiTaO₃ crystal protrudes beyond the coplanar probes and was situated above the device. The reflected light from the device active area partially struck the over hanging crystal. This, combined with the fact that the gate (Schottky diode) was illuminated, led us to believe that the disturbance of the photoresponse was caused by electromagnetic radiation emitted by the HEMT [14], [15]. To validate our hypothesis, the coplanar probe was removed from the drain and the vicinity of the device, while the crystal was maintained at its sampling position. A signal was detected with the drain floating and the gate biased relative to the source. Our measurements showed an increase in signal strength with increasing negative bias on the gate, in agreement with the findings of [14]. It was also discovered that by moving the location of the generation beam the signal strength was altered. This can be understood by realizing that the reflected beam struck the crystal at different positions as the generation beam was moved. These preliminary results support our electromagnetic radiation hypothesis. The ripple in the time-domain photoresponse tail is attributed to this phenomenon.

From the time-domain measurements, the relative power spectrum for both the lift-off and bulk devices was calculated. Given that the Fourier transform of the HEMT photoresponse is $Y_{\text{HEMT}}(\omega)$, the relative power spectrum is given by

$$P_{R,\text{HEMT}}(\omega) = 20 \log \left[\frac{Y_{\text{HEMT}}(\omega)}{Y_{\text{HEMT}}(0)} \right] \quad (2)$$

and is measured in decibels. $P_{R,\text{HEMT}}(\omega)$ is graphed in Fig. 6(a) up to 140 GHz for both sets of devices. The ripple in the relative power spectrum can be accounted for by the tail present in the time-domain photoresponse.

It is possible to roughly de-embed the effects of sampling condition 2 by using the calculated function $\zeta(\omega)$. The measured photoresponse is $Y_{\text{HEMT}}(\omega) = H_2(\omega)Q(\omega)$, where $Q(\omega)$ is the HEMT photoresponse at the contact pads. The adjusted response is

$$Y'_{\text{HEMT}}(\omega) = \frac{Y_{\text{HEMT}}(\omega)}{\zeta(\omega)} = H_1(\omega)Q(\omega). \quad (3)$$

In Fig. 6(b), the adjusted relative power spectrum is displayed.

The devices exhibit moderate frequency response up to 140 GHz. These results provided the motivation to optically heterodyne to 130 GHz. From Fig. 6(a) and (b), it is apparent that there is no significant degradation in the device photoresponse for the lift-off devices compared to the bulk devices. This is an encouraging result that provides validation for the integration of photonic and nonphotonic materials by the epitaxial lift-off process.

V. OPTICAL HETERODYNE TECHNIQUE

A. Theory of Optical Heterodyne

Optical heterodyne detection has been investigated by others to characterize the high-speed performance of photodetectors and optical receivers [16], [17]. This technique has the special advantages of being very broad-band and sensitive. The process involves the superposition and mixing of two laser beams in the device under test. Most simply, the interfering beams can be represented by two plane electromagnetic waves of frequency ω_1 and ω_2 . Assuming that they are collinear and have the same polarization, the resultant electric field of the two beams can be written as

$$E_t = E_1 \cos \omega_1 t + E_2 \cos \omega_2 t \quad (4)$$

where E_1 and E_2 are the electric field amplitudes of the incident beams. The device responds to the intensity of the incident light which is proportional to the square of the total electric field given by

$$E_t^2 = \frac{E_1^2}{2} + \frac{E_2^2}{2} + E_1 E_2 \cos(\omega_1 - \omega_2)t. \quad (5)$$

In deriving (5), the high-frequency term (sum) has been neglected. The total field generates photocurrents in our device which have both dc and ac components

$$i_{\text{total}} = i_{\text{dc}} + i_{\text{ac}} \\ = R_{\text{dc}} \left[\frac{E_1^2}{2} + \frac{E_2^2}{2} + F(\omega_b) \cdot E_1 E_2 \cos \omega_b t \right] \quad (6)$$

where R_{dc} is the dc responsivity of the device and $\omega_b = \omega_1 - \omega_2$ is the frequency of the beat signal. $F(\omega_b)$ is the frequency response of the device at ω_b and can be measured from dc to several hundreds of gigahertz by sweeping ω_b over the corresponding bandwidth. Such a sweep can be realized by using a frequency-tunable laser as a source for either of the two interfering optical signals. The quantum efficiency, η , is related to the change in dc photocurrent, i_{dc} , and the incident power, P_{inc} , by

$$\eta = \frac{h\nu}{q} \cdot \frac{i_{\text{dc}}}{P_{\text{inc}}} = \frac{h\nu}{q} \cdot R_{\text{dc}} \quad (7)$$

where h is Planck's constant, ν is the frequency of the incident radiation, and q is the electron charge.

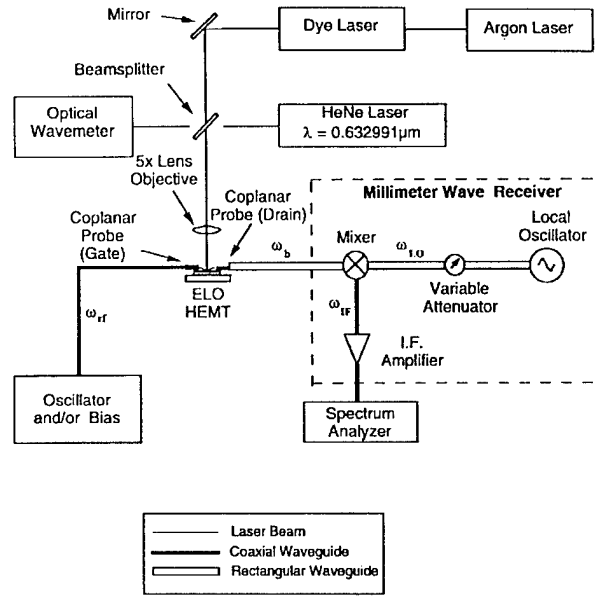


Fig. 7. Experimental setup of optical heterodyne measurements.

B. Optical Heterodyne Measurements

The experimental setup of our optical heterodyne measurements is shown in Fig. 7. A temperature-stabilized single-mode He-Ne laser (0.5 mW) with a linewidth of less than 1 MHz was employed as the source for the fixed frequency optical signal. A CW ring dye laser (Coherent CR 699-21, 300 mW) optically pumped by an argon laser was used as a tunable source for the local oscillator signal. A variable attenuator was used to reduce the dye power incident on the device. The dye laser was actively stabilized and servo-locked to an oven-stabilized Fabry-Perot interferometer by an external feedback mechanism. This ensured highly stable, mode-hop-free single-mode laser operation with a linewidth less than 0.5 MHz and a long-term frequency drift of less than 50 MHz/h. The dye laser was continuously tunable over the whole dye spectrum and could be linearly scanned over tens of gigahertz in its locked mode of operation. Kiton Red (600–640 nm) was used as the dye gain medium, ensuring hundreds of gigahertz of tunability around the HeNe wavelength (632.991 nm). Because of the very narrow linewidths and stability of the lasers, extremely sensitive optical heterodyne measurements on high-speed devices could be performed.

The two laser beams were combined and made collinear by a beam splitter. The combined beam was focused on the device under test by a 5× objective lens. A fraction of the dye laser beam was fed to a wavemeter (Burleigh) for continuous monitoring of the dye wavelength. The wavemeter, which has a resolution of 0.001 nm, allowed us to set the dye wavelength to an accuracy of less than 1 GHz for a given frequency offset from the HeNe. This gave us a rough estimate of the difference frequency generated by our mixing.

High-frequency coplanar probes and bias tees were used to make contact and dc bias the HEMT devices. The probes also acted as broad-band well-matched antennas. The millimeter wave signals generated in our devices were radiated and

TABLE I
OPTICAL HETERODYNE SNR OF THE LIFT-OFF
AND BULK HEMT'S AT 60, 94, AND 130 GHz

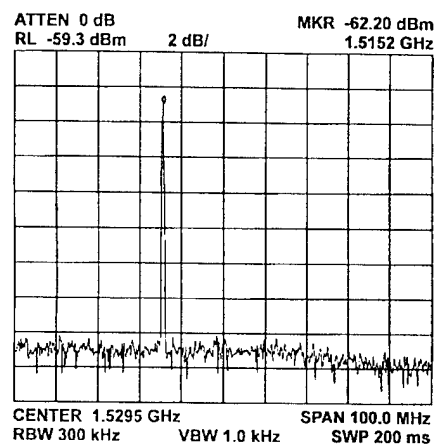
Frequency (GHz)	SNR for Lift-off HEMT (dB)	SNR for Bulk HEMT (dB)
60	19.3	21.4
94	14.0	14.2
130	8.2	10.7

launched into waveguides through the probes. This is equivalent to radiating the signal by an integrated antenna structure and receiving the signal with a collecting horn. This opens up the possibility of using these devices as compact optically driven millimeter wave sources. Our experiments used a heterodyne detection scheme to downconvert the optically generated millimeter wave signals. The signal from the device was combined with a local oscillator using a directional coupler and then fed to a commercial mixer. The IF signal from the mixer was amplified and then displayed on a spectrum analyzer.

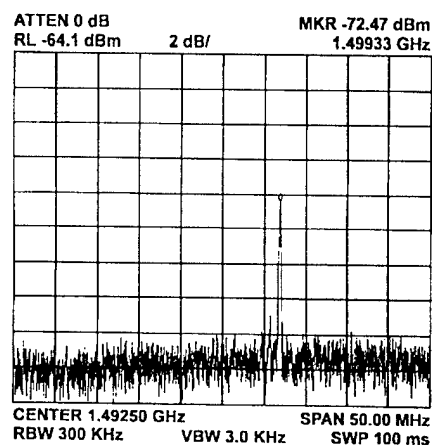
The lift-off devices showed dc responsivities of 4.2 A/W and a quantum efficiency of 825% when illuminated with the HeNe. Our optical heterodyne measurements were done at 60, 94, and 130 GHz on the HEMT's before and after lift-off. The results of these measurements are outlined in Table I. The spectrum analyzer traces of the 94-GHz and 130-GHz downconverted beat signals are shown in Fig. 8(a) and (b), respectively. As can be seen, both lift-off and bulk HEMT's have comparable performance within experimental errors. The process of lift-off has not produced any observable degradation in the optical response characteristics. In Table I, the appropriate bias was used to maximize the SNR for each frequency point.

It should be noted that in this table the data between frequency points is not calibrated. This is due to the fact that differences existed between the probing setup and the millimeter wave detection scheme for each frequency point. In the 60-GHz experiment, two 67-GHz coplanar probes (Picoprobe Model 67A) with V-connector outputs were employed at the drain and gate terminals. The drain output was fed into the mixer via a coaxial to a waveguide transition. The local oscillator was a tunable 60-GHz GUNN oscillator. In the 94-GHz experiment, a different coplanar probe (Picoprobe Model 120) was employed at the drain side. This probe has a built-in coplanar to W-band waveguide transition which enabled us to couple the optically generated signal directly into the mixer. A 94-GHz tunable reflex klystron was used for the local oscillator.

The detection of radiation with frequencies extending beyond the bandwidth of the coplanar probes (120 GHz) could



(a)



(b)

Fig. 8. Optical heterodyne signal of the lift-off HEMT after downconversion of the (a) 94-GHz and (b) 130-GHz signals as seen on a spectrum analyzer. This data is also tabulated in Table I.

not be achieved with heterodyne detection as described above. This led us to devise a different detection scheme involving three-wave mixing for the 130-GHz measurements. In this scheme, a microwave or millimeter wave signal of frequency ω_{rf} was applied to the gate of the HEMT while it was illuminated with the two optical beams. The mixing of these three signals took place in the device. This process took advantage of the nonlinearity of the HEMT current-voltage characteristics to generate mixing products between the optically generated current at the difference frequency (ω_b) and the current component injected at the gate (ω_{rf}). One of the mixing products generated has a frequency $\omega_b - \omega_{rf}$ ($= \omega_1 - \omega_2 - \omega_{rf}$). By using an appropriate ω_{rf} , the frequency of the mixing product can be adjusted to a frequency (within the bandwidth of the probes) that could be radiated into the heterodyne receiver system.

The use of three-wave mixing to detect optical heterodyne signals in photoconductors was demonstrated in [17]. There the measurements involved frequencies less than a gigahertz, although the possibility of using this method beyond 100 GHz with a similar device made from a high-speed material was mentioned. The viability of this approach and the ability

of the HEMT to act as a high-speed three-wave mixer was demonstrated. Using this technique, high-frequency signals ranging up to 240 GHz can be detected with more readily available low-frequency sources.

In our experiments, a 130-GHz signal was optically generated in the HEMT and mixed with a 35-GHz signal applied to the gate. A klystron was used as a source for this gate signal. The 94-GHz output signal was launched into a waveguide and subsequently heterodyne detected in our millimeter wave detector. The local oscillator used for the final downconversion was a tunable 95-GHz GUNN oscillator. It is interesting to note that we also were able to observe the sum frequency of the mixing between the optically generated current and the injected gate current at 94 GHz ($\omega_b + \omega_{rf}$) by simply tuning the optical difference frequency from 130 to 60 GHz. This signal was approximately 5 dB larger than our 130-GHz signal.

Sensitive optical response measurements to 130 GHz on ELO HEMT's using heterodyne techniques has been demonstrated. Although measurements were conducted at only three discrete frequencies, it is possible to sweep the frequency in order to obtain a complete spectrum of the HEMT photoresponse. Our measurements confirm the ability to optically generate high-frequency signals in three terminal devices. This lends itself to the possibility of making compact millimeter wave sources using optically driven ELO HEMT's and semiconductor lasers.

VI. CONCLUSION

We have successfully measured the optical response of 1- μm ELO HEMT photodetectors to modulation frequencies of 140 GHz using both electrooptic sampling and optical heterodyne techniques. Our picosecond results demonstrate that lift-off devices can be used at millimeter wave frequencies with no degradation in response. Optical heterodyne experiments at 60, 94, and 130 GHz provided further confirmation of this. These results indicate the enormous potential of the epitaxial lift-off process in the integration of millimeter wave optoelectronic integrated systems. Current efforts in this area include testing at 1.3 μm for applications in communication systems, performing a fully calibrated optical heterodyne response to 150 GHz, and characterizing the effect of the illumination level on the millimeter wave response of high-frequency devices. These latest efforts will focus on 0.1- μm and 50-nm gate HEMT photodetectors which have f_T 's of 170 and 340 GHz, respectively.

APPENDIX

For millivolt-level electrical transients under typical sampling conditions, the electrooptic signal is weak. A differential

detection method can be employed to enhance the SNR. Operationally, in matching the detection system there will be a small imbalance, ψ , caused by variations in photodiode load, responsivity, and illumination ($0 < \psi < 1$). Due to this imbalance, laser amplitude noise and Shot and/or Johnson noise will contribute to the degradation of the SNR. When the generation beam is amplitude modulated for signal detection purposes, modulated laser amplitude noise will also cause a degradation in SNR.

For the detection system used in this paper, the SNR is defined in (A1), shown at the bottom of the page, where V_o is the peak-peak voltage drop across the crystal, V_{avg} is the voltage drop across a photodiode load due to the sampling beam average power, $|V_n(f)|^2$ is the power spectral density arising from Shot and/or Johnson noise, $|N(f)|^2$ is the spectral density of the laser amplitude noise, f_m is the frequency at which the generation beam is modulated, and Δf is the bandwidth of the detection system (limited by the LIA). In deriving (A1), it was assumed that $|N(f)|^2$ does not vary significantly across the detection bandwidth [8]. In the denominator of (A1), the first two terms correspond to the laser amplitude noise power and the Shot and/or Johnson noise power, respectively, while the third term represents the modulated laser amplitude noise power.

Assuming small $|V_n(f)|^2$, $\psi \gg 2V_o/V_\pi$, and in the limit of low modulation frequencies such that $|N(f)|^2 \approx |N(f - f_m)|^2$, the SNR is dominated by the laser amplitude noise and can be simplified to

$$\text{SNR} \approx \frac{V_o^2}{\left(\frac{\psi V_\pi}{2}\right)^2 |N(f)|^2 \Delta f} \quad (\text{A2})$$

According to (A2), the SNR can be improved by increasing the modulation frequency provided there is an imbalance in the detection system. However, this trend cannot be maintained indefinitely. When the modulation frequency is such that $(|N(f_m)|/|N(0)|)^2 = (2V_o/\psi V_\pi)^2$, the modulated laser amplitude noise contributes the same amount of power as the laser amplitude noise. Beyond this point, the efficacy of increasing the modulation frequency begins to decrease.

The effect of the modulation frequency on the SNR can be judged from the ratio of the modulated laser amplitude noise power to the power of the other noise sources which we call ϑ . Experimentally this ratio can be determined by first measuring the noise power level with a voltage applied to the coplanar probe and subsequently with no voltage applied. We define this ratio as γ^2 and is related to ϑ by (A3), shown at the top of the next page. With a 481-mV signal applied to the coplanar probe and for our sampling conditions, $\gamma = 1.979$. In this case,

$$\text{SNR} \approx \frac{2 \left(\frac{V_{\text{avg}}}{V_\pi} \right)^2 V_o^2}{\left(\frac{(\psi V_{\text{avg}})^2}{2} |N(f)|^2 + 2 |V_n(f)|^2 + 2 \left(\frac{V_{\text{avg}}}{V_\pi} \right)^2 V_o^2 |N(f - f_m)|^2 \right) \Delta f} \quad (\text{A1})$$

$$\gamma^2 = \frac{\frac{(\psi V_{avg})^2}{2} |N(f)|^2 + 2|V_n(f)|^2 + 2\left(\frac{V_{avg}}{V_\pi}\right)^2 V_o^2 |N(f - f_m)|^2}{\frac{(\psi V_{avg})^2}{2} |N(f)|^2 + 2|V_n(f)|^2} = \vartheta + 1 \quad (A3)$$

the modulated laser amplitude noise power is approximately three times larger than the laser amplitude and Shot and/or Johnson noise power combined.

ACKNOWLEDGMENT

The authors would like to thank W. Chang for technical assistance with the lift-off process, Dr. M. Y. Frankel for insightful discussions on the electrooptic sampling setup, and G. Boll of Picoprobe for technical assistance with the coplanar probes.

REFERENCES

- [1] D. M. Shah, W. K. Chan, T. J. Gmitter, L. T. Florez, H. Schumacher, and B. P. Van der Gaag, "DC and RF performance of GaAs MESFET fabricated on silicon substrate using Epitaxial lift-off technique," *Electron. Lett.*, vol. 26, no. 22, pp. 1865-1866, Oct. 1990.
- [2] F. Kobayashi and Y. Sekiguchi, "GaAs Schottky photodiode fabricated on glass substrate using epitaxial lift-off technique," *Jpn. J. Appl. Phys.*, vol. 31, no. 7A, pp. L850-L852, July 1992.
- [3] V. Arbet-Engels, W. Chang, E. Yablonovich, G. J. Sullivan, M. K. Swed, and M. F. Chang, "Flexible, thin-film, GaAs hetero-junction bipolar transistors mounted on natural diamond substrates," *Solid State Electron.*, vol. 38, no. 11, pp. 1972-1974, 1995.
- [4] D. Bhattacharya, P. S. Bal, H. R. Fetterman, and D. Streit, "Optical mixing in epitaxial lift-off pseudomorphic HEMT's," *IEEE Photon. Technol. Lett.*, vol. 7, pp. 1171-1173, 1995.
- [5] P. G. Young, S. A. Alterovitz, R. A. Mena, and E. D. Smith, "RF properties of epitaxial lift-off HEMT devices," *IEEE Trans. Electron Devices*, vol. 40, pp. 1905-1909, Nov. 1993.
- [6] E. Yablonovich, D. M. Hwang, T. J. Gmitter, L. T. Florez, and J. P. Harbison, "Van der Waals bonding of GaAs epitaxial films onto arbitrary substrates," *Appl. Phys. Lett.*, vol. 56, pp. 2419-2421, June 1990.
- [7] J. A. Valdmanis, "1 THz-Bandwidth probe for high-speed devices and integrated circuits," *Electron. Lett.*, vol. 23, no. 24, pp. 1308-1310, 1987.
- [8] B. H. Kolner, "Picosecond electro-optic sampling in Gallium Arsenide," Ph.D. dissertation, Stanford University, Stanford, CA, 1985.
- [9] M. Y. Frankel, J. F. Whitaker, G. A. Mourou, and J. A. Valdmanis, "Experimental characterization of external electrooptic probes," *IEEE Microwave Guided Wave Lett.*, vol. 1, pp. 60-62, 1991.
- [10] T. Nagatsuma, T. Shibata, E. Sano, and A. Iwata, "Subpicosecond sampling using a noncontact electro-optic probe," *J. Appl. Phys.*, vol. 66, no. 9, pp. 4001-4009, 1989.
- [11] J. M. Chwalek and D. R. Dykaar, "A mixer based electro-optic sampling system for submillivolt signal detection," *Rev. Sci. Instrum.*, vol. 61, no. 4, pp. 1273-1276, 1990.
- [12] M. Z. Martin, F. K. Oshita, M. Matloubian, H. R. Fetterman, L. Shaw, and K. L. Tan, "High-speed optical response of pseudomorphic InGaAs high electron mobility transistors," *IEEE Photon. Technol. Lett.*, vol. 4, pp. 1012-1014, 1992.
- [13] F. K. Oshita, "Picosecond optoelectronic characterization of ballistic electron transistors," Ph.D. dissertation, Univ. California at Los Angeles, 1992.
- [14] L. Xu, X. C. Zhang, D. H. Auston, and B. Jalali, "Terahertz radiation from large aperture Si p-i-n diodes," *Appl. Phys. Lett.*, vol. 59, no. 26, pp. 3357-3359, 1991.
- [15] X. C. Zhang, B. B. Hu, J. T. Darrow, and D. H. Auston, "Generation of femtosecond electromagnetic pulses from semiconductor surfaces," *Appl. Phys. Lett.*, vol. 56, no. 11, pp. 1011-1013, 1990.
- [16] R. T. Hawkins, II, M. D. Jones, S. H. Pepper, and J. H. Goll, "Comparison of fast photodetector response measurements by optical heterodyne and pulse response techniques," *J. Lightwave Technol.*, vol. 9, pp. 1289-1294, 1991.

- [17] J. K. A. Everard, "Novel coplanar three wave mixer for coherent and heterodyne detection of optical signals," *Electron. Lett.*, vol. 24, no. 14, pp. 883-885, 1988.



interactions in solid-state devices and integration techniques for optoelectronic circuits and devices.

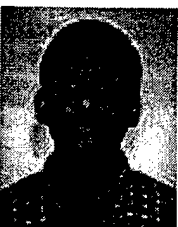


Daipayan Bhattacharya was born in Chandernagore, India, in November 1969. He received the B.S. and M.S. degrees in electrical engineering from the University of California, Los Angeles (UCLA), in 1990 and 1994, respectively. He is currently pursuing the Ph.D. degree in electrical engineering at UCLA.

From 1990 to 1994, he was a Member of the Technical Staff in the Radar Laboratory at Hughes Missile Systems Group, Canoga Park, CA. His research interests include optical-millimeter wave

Hernan Erlig was born in Buenos Aires, Argentina, in 1969. He received the B.S. and M.S. degrees in electrical engineering from the University of California, Los Angeles (UCLA), in 1992 and 1996, respectively. He is currently pursuing the Ph.D. degree in electrical engineering.

His research interests include high-frequency characterization techniques for devices, ultrafast phenomena, device physics, and high-temperature superconductivity.



Mohammed E. Ali was born in Lalmonirhat, Bangladesh, in December 1967. He received the B.Sc. degree in electrical and electronic engineering from Bangladesh University of Engineering and Technology (BUET) in 1992 and the M.S. degree in electrical engineering from the University of California, Los Angeles (UCLA), in 1997. His thesis involved high-frequency optical mixing in three-terminal devices. He is currently pursuing the Ph.D. degree at UCLA.

From 1992 to 1994, he was a Lecturer with the Department of Electrical and Electronic Engineering, BUET. His research interests include generation of millimeter waves and characterization of high-speed devices using optical techniques.



Shamino Wang was born in Taiwan in 1969. He received the B.S. degree in physics from the National Tsing Hua University, Taiwan, in 1992 and the M.S. degree in physics from the University of California, Los Angeles (UCLA), in 1994. He is currently pursuing the Ph.D. degree in physics at UCLA.

His research interests include CDMA optical fiber communication networks and microwave generation from common-ring cavity Brillouin lasers in optical fibers.



Harold R. Fetterman (SM'81-F'90) received the B.A. degree in physics from Brandeis University, Waltham, MA, in 1962 and the Ph.D. degree from Cornell University, Ithaca, NY, in 1967.

After joining Lincoln Laboratory, Massachusetts Institute of Technology, Cambridge, he began to investigate new solid-state high-frequency devices. This included FET's, HEMT's, HBT's, quantum-well structures, and resonant tunneling structures. In 1982, he joined the University of California, Los Angeles (UCLA) Electrical Engineering Department

as a Professor and First Director of the Center for High Frequency Electronics. During this period, he also became active in studying optoelectronics and optical control of millimeter wave devices. Currently, he has programs in investigating new polymer optical modulators, millimeter wave device concepts, and novel means of testing using laser techniques. He has helped organized many new activities including the Optically Controlled Phased Array Radar Project in the National Center for Integrated Photonics.



Richard Lai was born in Evanston, IL, in 1964. He received the B.S.E.E. degree from the University of Illinois Urbana-Champaign in 1986 and the M.S.E.E. and Ph.D. degrees from the University of Michigan, Ann Arbor, in 1988 and 1991, respectively.

He joined TRW's Advanced Microelectronics Laboratory, TRW Electronic Systems and Technology Division, Redondo Beach, CA, in 1991 as a Product Engineer, where he has been involved in the research, development, and insertion of advanced

GaAs-based and InP-based HEMT device and MMIC technologies into various military and commercial MMW applications. In 1994, he became the Principal Investigator for an advanced HEMT research and development project at TRW and has been heavily involved in supporting advanced HEMT MMIC production on TRW's flexible manufacturing line. He has authored and co-authored over 40 papers and conference presentations in the area of advanced GaAs and InP-based device and circuit technology.



Dwight C. Streit (S'85-M'86-SM'92) received the Ph.D. degree in electrical engineering from the University of California, Los Angeles, in 1986.

He has since been with TRW's Electronic Systems and Technology Division, Redondo Beach, CA, where he is currently Assistant Manager of the Micro Electronics Product and Technology Development Department. He is a TRW Technical Fellow and Principal Investigator for several research and development projects related to III-V materials, monolithic HEMT-HBT integrated circuits, and quantum effect devices.

Optical mixing to 211 GHz using 50 nm gate pseudomorphic high electron mobility transistors

M. E. Ali, D. Bhattacharya, and H. R. Fetterman

Department of Electrical Engineering, University of California, Los Angeles, California 90095

M. Matloubian

Hughes Research Laboratories, Malibu, California 90265

(Received 5 June 1997; accepted for publication 24 November 1997)

We report optical mixing with difference frequencies to 211 GHz in 50 nm gate pseudomorphic InP-based high electron mobility transistors (HEMTs). To our knowledge, this is the highest frequency optical mixing signal obtained in three terminal devices. To detect the signals at these frequencies, a novel three-wave-mixing configuration was employed. To demonstrate the wide tunability of this setup, a sweep of frequencies from 160 to 190 GHz was performed. The optically generated millimeter wave signals were downconverted to 97 GHz and radiated. For the radiation experiments, tunable baseband signals were also added by injection into the gate terminal of our HEMTs, thereby providing a method to transmit information. © 1998 American Institute of Physics. [S0003-6951(98)02404-8]

Optical mixing is a promising technique to generate continuously tunable millimeter wave frequencies. The generated signals are of high quality in terms of stability, noise, and spectral purity. Combined with optical fiber technology, this technique has applications in many important areas including phased array radar, remote sensing, spectroscopy and communications where optical fibers can serve as efficient, low loss transport, and distribution media. For photodetector applications, two-terminal devices have been mostly used, although three-terminal devices such as high electron mobility transistors (HEMTs)^{1,2} and heterojunction bipolar transistors^{3,4} are becoming increasingly competitive, due to their inherent gain. The presence of a third terminal also adds a degree of freedom in controlling the mixing process. In particular, the gate can be employed to introduce a baseband information signal for upconversion to a millimeter wave carrier, which is optically generated in the same device.

Recently, we have demonstrated optical mixing with difference frequencies to 130 GHz in 1 μm gate-length epitaxial liftoff HEMTs.⁵ In this letter, we report the extension of this mixing to a record high of 211 GHz using 50 nm gate pseudomorphic AlInAs/GaInAs/InP HEMTs. The high frequency optically generated signals are detected using a broadband three-wave mixing technique. A sweep over the frequency range of 160–190 GHz was performed to demonstrate the tunability of our heterodyne system.

In our second set of experiments, 97 GHz optically generated signals were radiated into free space by way of a coplanar-to-waveguide transition and a radiating horn. The 210 GHz mixed signals were also radiated after downconversion to 97 GHz. This demonstration validated the concept that by using suitable antenna structures integrated with the device, these high frequencies could be directly radiated. Further integration with semiconductor lasers can be a cost effective way of making compact optoelectronic millimeter wave sources. Enabling integration techniques, such as epitaxial liftoff and integrated slot antennas, are being investigated for such applications.⁶ Finally, using the gate terminal, tunable electrical sidebands were superimposed on the 97

GHz optically generated signal and then radiated into free space to demonstrate transmission of information using fiber-millimeter wave links.

The devices used in our experiments were 50 nm gate-length delta-doped pseudomorphic AlInAs/GaInAs/InP HEMTs.^{7,8} The structure had a sheet-charge density of approximately $2.7 \times 10^{12} \text{ cm}^{-2}$ and a channel mobility of approximately $13\,000 \text{ cm}^2/\text{Vs}$ at 300 K. On wafer electrical characterization of the devices was performed on a HP8510C vector network analyzer from 0 to 50 GHz. A millimeter wave extension kit utilizing frequency multipliers and external harmonic mixers was also used to further extend the s -parameter measurements to W band (75–110 GHz). The short circuit current gain and unilateral power gain for our HEMTs are shown in Fig. 1. The device was biased at $V_{\text{DS}}=0.7 \text{ V}$ and $V_{\text{GS}}=0.0 \text{ V}$. The devices showed excellent gain response characteristics. A cutoff frequency, f_T of 228 GHz and a maximum oscillation frequency, f_{max} of 124 GHz were obtained from extrapolation of the measured gain characteristics.

The dc responsivity and quantum efficiency for our devices were measured to be 74 A/W and 145, respectively. The overall responsivity was 2 A/W when external coupling losses were included. The coupling efficiency was estimated to be 2.7%. Quantum efficiencies greater than 100% can be achieved, since in HEMTs the photogenerated holes participate in a current gain mechanism that results in an injection of additional electrons in the channel layer.

In our optical mixing experiments, the HEMT was illuminated with two collinear optical beams with a desired frequency offset. The mixing current at the difference frequency, ω_b is

$$i_{\text{ac}}(t) = 2F(\omega_b)\sqrt{P_1 P_2} \cos(\omega_b t), \quad (1)$$

where $F(\omega_b)$ is the ac responsivity of the device, P_1 and P_2 are incident optical powers. The high frequency limit of the mixing process is set by the dynamic photoresponse, $F(\omega_b)$ of the device.

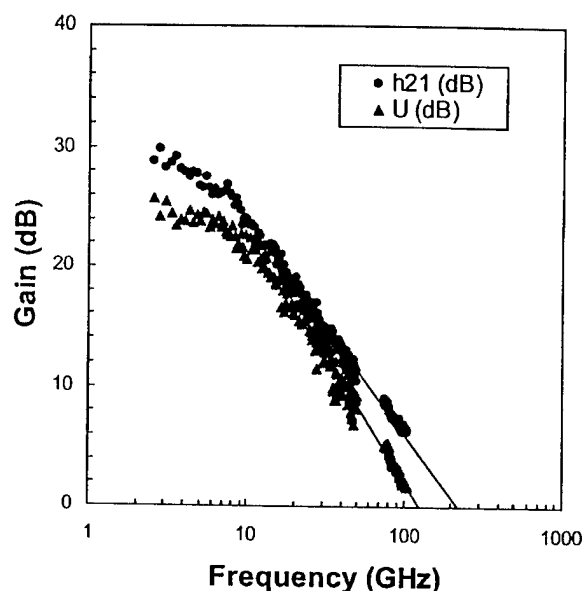


FIG. 1. Electrical gain measurements (unilateral power gain, U , and short-circuit current gain, h_{21}) for the HEMTs were performed on an extended 8510C vector network analyzer from 0 to 50 GHz and 75–110 GHz. From extrapolation of the data, f_{\max} is found to be 124 GHz and f_T is found to be 228 GHz.

The signal and local oscillator fields used in our optical mixing experiments were obtained from a temperature stabilized single frequency HeNe laser and an Argon pumped continuous wave ring dye laser, respectively. The dye laser was operated with Kiton Red 620 dye (600–640 nm) and had the capability to tune mechanically hundreds of GHz, and electronically 30 GHz around the wavelength of HeNe (632.991 nm). The optical power incident on the device from the HeNe was 0.5 mW. A variable attenuator was used in the dye laser path to limit the incident dye laser power on the device to a few milliwatts. The incident dye laser power was kept low to avoid saturation of the device and to obtain good modulation depth. A 5X objective lens was used to focus the optical radiation on the device in this free space implementation. Fiber optic connections have also been demonstrated and will be used in our next extension to submillimeter wave frequencies.

To contact our devices, we used high frequency commercial coplanar probes and bias tees. The probes, which were coupled to waveguides, acted as well matched antennas for our devices throughout W band. To overcome the bandwidth limitations imposed by use of the probes, a three-wave mixing technique was employed. For this configuration, a millimeter wave signal of frequency ω_g was injected into the gate of the device. The interaction between the modulation induced by this signal and the optically generated signal produced a down-converted signal of frequency $\omega_{rf} = \omega_b - \omega_g$, as well as other mixing products. The frequency of the gate signal was chosen such that ω_{rf} fell within the detection bandwidth of our external receiver system. A backward wave oscillator (BWO) tunable over the entire band was used as a millimeter wave source for the gate signal.

The three-wave mixing technique took advantage of the multifunction capability of the HEMTs. The interaction of two optical waves and an electrical signal injected into the

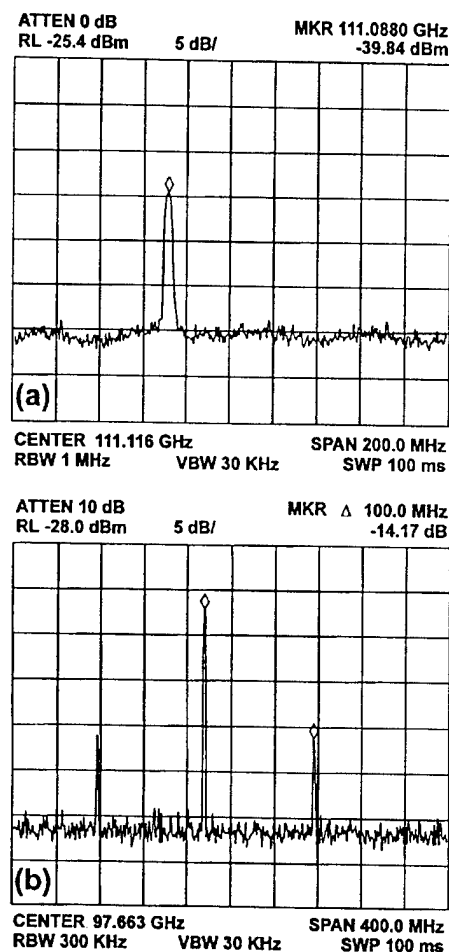


FIG. 2. (a) Spectrum analyzer trace of the 211 GHz optically generated signal which has been downconverted to 97 GHz in the HEMTs and heterodyne detected in our millimeter wave receiver. (b) Baseband information signals imposed on a 97 GHz optically generated carrier by injection into the gate terminal of our device.

gate can be considered as a hybrid of two different processes, optical mixing, and electrical down-conversion. The first process makes use of the quadratic response of the device to coherent optical fields, as described in Eq. (1). The optically generated current is then modulated by the injected electrical gate signal, producing a sum and difference frequency component:

$$\begin{aligned} i(t) &= 2F(\omega_b)\sqrt{P_1P_2}\cos(\omega_bt)A\cos(\omega_gt) \\ &= AF(\omega_b)\sqrt{P_1P_2}[\cos(\omega_b + \omega_g)t + \cos(\omega_b - \omega_g)t]. \end{aligned} \quad (2)$$

Our millimeter wave receiver filters the sum component and detects the difference frequency for display on a spectrum analyzer.

Both mixing processes were observed to be strongly dependent on the operating bias point. The strength of the optical mixed signal depends upon the photocurrents present in the active layer. This mixing photocurrent was usually optimized by operating the device at a higher drain voltage and at a gate voltage close to zero. On the other hand, efficient down-conversion is obtained when the device nonlinearity is more pronounced. This usually happens when the device is

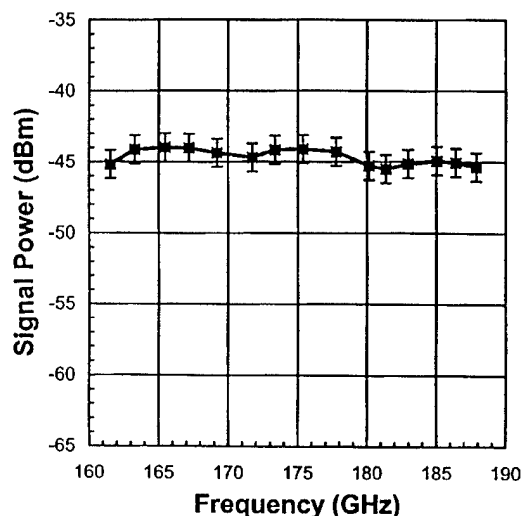


FIG. 3. Swept frequency optical heterodyne measurements on the HEMTs from 160 to 190 GHz, demonstrating the wide tunability of our system.

biased at drain voltage just before the onset of saturation. Therefore a compromise has to be made in choosing the bias point when the two processes are occurring simultaneously.

In our first set of measurements, we detected an optical mixed signal at 211 GHz in our HEMTs with the BWO frequency set to 114 GHz. The down-converted 97 GHz signal was radiated and launched into the waveguide input of the external receiver system using the coplanar probes as antenna elements, as described above. A spectrum analyzer trace of the signal is shown in Fig. 2(a). A 16 dB signal-to-noise ratio was achieved with the device's bias optimized at $V_{DS}=0.6$ V and $V_{GS}=0.1$ V.

To demonstrate the wide tunability of our optical mixing signal, we performed a sweep from 160 to 190 GHz. In order to minimize the effect of the external receiver system on our measurements, the frequency of the down-converted signal in the device was kept constant at 76 GHz throughout the sweep by simultaneously tuning the dye laser frequency and the BWO frequency. The BWO power applied to the gate and the incident optical power were also kept constant while tuning. The device was biased at $V_{DS}=0.7$ V and $V_{GS}=-0.2$ V. The response of the device is shown in Fig. 3. The excellent response suggests that these devices can be used to generate frequencies much higher than 211 GHz by optical mixing.

Having demonstrated high frequency optical mixing we then examined the radiation and propagation of the optically generated signals in free space. In this set of measurements, the optically generated millimeter waves were fed to a radiating horn antenna via the coplanar probes. The free space radiation was then collected using a horn antenna and de-

tected in our millimeter wave receiver system. Initially, an optical beat signal of 97 GHz was generated in the device and radiated. The signal-to-noise ratio of the detected signal was 24 dB. The 211 GHz optical mixed signal was also generated, downconverted to 97 GHz, and then radiated. In this case, a signal-to-noise ratio of 12 dB was achieved. This validates the use of these devices as compact optically controlled millimeter wave sources. Future integration with on wafer antennas using epitaxial liftoff technology is currently being pursued to radiate the 211 GHz signals directly.

Lastly, to demonstrate the viability of transferring information using our heterodyne system in an optical-millimeter wave link, a 100 MHz rf signal was imposed on a 97 GHz optically generated carrier. To impress the information signal on the carrier it was injected into the gate of the HEMT. This highlights a unique advantage of using three-terminal devices over two-terminal devices for optical-millimeter wave applications. The modulated millimeter wave signal was then radiated into free space as described above and collected in our heterodyne receiver. The detected signal is shown in Fig. 2(b). The sidebands were 14.2 dB down from the carrier for a rf signal power of 0 dBm. The rf signal frequency was swept over a few hundred MHz and no appreciable change in sideband strength was observed.

In conclusion, we have demonstrated the mixing of two continuous wave laser beams in 50 nm gate pseudomorphic HEMTs to generate continuously tunable mixed signals to 211 GHz. A sweep performed over the frequency range from 160 to 190 GHz indicated that these devices have excellent optical response characteristics. Optically generated signals, both continuous wave and modulated, were radiated into free space at 97 GHz using a horn.

This work was supported by the Air Force Office of Scientific Research under the direction of H. R. Schlossberg, by the National Center for Integrated Photonics Technology, and by a University of California MICRO Grant.

¹D. Bhattacharya, M. E. Ali, H. R. Fetterman, and D. Streit, Conference Proceedings of the 9th Annual Meeting of the IEEE Lasers and Electro-Optics Society (1996), Vol. 2, p. 326.

²M. A. Romero, M. A. G. Martinez, and P. R. Herczfeld, IEEE Trans. Microwave Theory Tech. **44**, 2279 (1996).

³D. C. Scott, D. V. Plant, and H. R. Fetterman, Appl. Phys. Lett. **61**, 1 (1992).

⁴L. E. M. de Barros, A. Paoletta, P. R. Herczfeld, and A. A. de Salles, IEEE MTT-S International Microwave Symposium Digest **3**, 1445 (1996).

⁵D. Bhattacharya, H. Erlig, M. E. Ali, S. Wang, H. R. Fetterman, R. Lai, and D. Streit, IEEE J. Quantum Electron. **33**, 1507 (1997).

⁶D. Bhattacharya, P. S. Bal, H. R. Fetterman, and D. Streit, IEEE Photonics Technol. Lett. **7**, 1171 (1995).

⁷L. D. Nguyen, A. S. Brown, M. A. Thompson, and L. M. Jelloian, IEEE Trans. Electron Devices **39**, 2007 (1992).

⁸S. E. Rosenbaum, B. K. Kormanyos, L. M. Jelloian, M. Matloubian, A. S. Brown, L. E. Larson, L. D. Nguyen, M. A. Thompson, L. P. B. Katehi, and G. M. Rebeiz, IEEE Trans. Microwave Theory Tech. **43**, 927 (1995).

High-Frequency Polymer Modulators with Integrated Finline Transitions and Low V_π

Datong Chen, Daipayan Bhattacharya, Anand Udupa, Boris Tsap, Harold R. Fetterman, *Fellow, IEEE*, Antao Chen, Sang-Shin Lee, Jinghong Chen, William H. Steier, *Fellow, IEEE*, and Larry R. Dalton

Abstract—Ultra-high-speed integrated electrooptic polymer phase modulators have been fabricated and tested. They are made from a new nonlinear optical polymer, amino phenylene isophorone isoxazolone (APII), and are incorporated with integrated high-speed electrode transitions for W -band (75–110 GHz) operation. This new polymer has also been used to fabricate Mach-Zehnder modulators. These devices show good performance over a wide frequency band ranging to 40 GHz and have a $V_\pi < 10$ V. The measurements establish APII, and other chromophores specially designed to minimize chromophore–chromophore interaction, as strong contenders for fabricating modulators for commercial and military applications.

Index Terms—Electrooptic modulation, finline transition, optical mixing, optical waveguides, traveling-wave devices.

NONLINEAR optical polymer materials have become a viable option for future high-performance integrated optics. This is especially true for high-frequency optical circuits because of their high nonlinearity, fast electronic response and near ideal velocity match for traveling-wave devices. Recent progress in research on nonlinear optical polymer materials and devices made from them confirm these predictions [1]–[4].

Previously, we demonstrated the operation of polymer traveling-wave phase modulators up to 110 GHz [5]. In those experiments, we used commercial coplanar waveguide probes (Picoprobe Model 120) to launch the driving power into the modulators. Though these probes provided excellent coupling of the power up to 120 GHz, they are unsuitable for integrated modulator structures due to their cost, size, and geometry. In this paper, we present the design and fabrication of a set of devices with monolithically integrated antipodal finline transitions, the structure of which is shown in Fig. 1. It has the advantage of low loss and high-dimensional fabrication tolerance. The transition gradually transforms the electric field

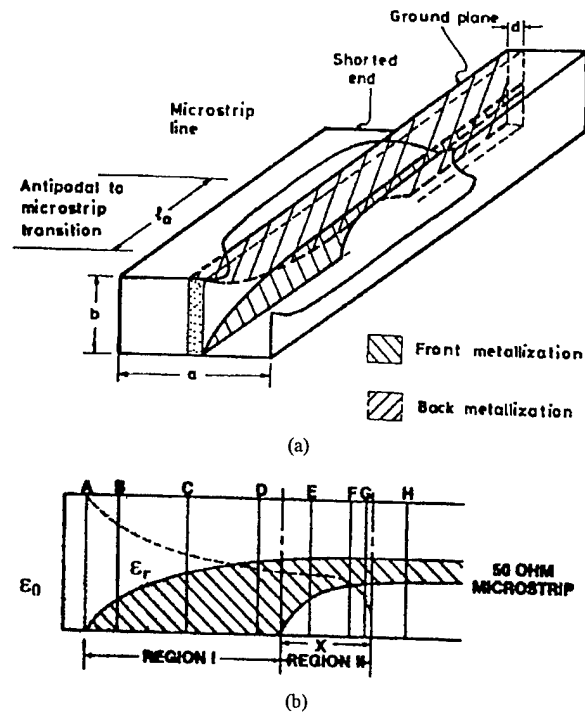


Fig. 1. (a) Design of the finline transition. (b) The changing overlap between the top and bottom electrodes gradually rotates the electric field by 90° .

profile of the rectangular metallic waveguide to that of the microstrip line electrode on the device and effectively couples the microwave driving power into the modulator.

We chose to use a $127\text{-}\mu\text{m}$ -thick Mylar film as the dielectric substrate owing to its low microwave loss tangent; good electrical, chemical, thermal and mechanical properties. The Mylar film was glued onto a silicon wafer for mechanical support during processing and detached from it just before insertion into the waveguide. A layer of silver and gold was deposited on the Mylar to serve as the lower ground plane for the microstrip lines.

Using photolithography, the lower finline transition pattern was etched in the region to be inserted into the waveguide. The lower cladding layer and the active polymer layer were spin coated and the active polymer was corona poled. The optical waveguide pattern was defined on the polymer using reactive ion etching with alignment to the pre-etched ground pattern. The upper cladding was spun on and a thin layer of chromium and gold was deposited for the top electrode.

Manuscript received August 3, 1998; revised September 15, 1998. This work was supported by the Air Force Office of Scientific Research and by the Office of Naval Research.

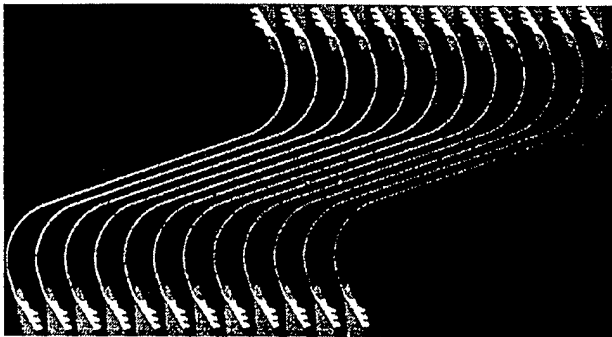
D. Chen was with the Department of Electrical Engineering, University of California, Los Angeles, CA 90095 USA. He is now with Hewlett-Packard Laboratory, Palo Alto, CA 94304 USA.

D. Bhattacharya, A. Udupa, and H. R. Fetterman are with the Department of Electrical Engineering, University of California, Los Angeles, CA 90095 USA.

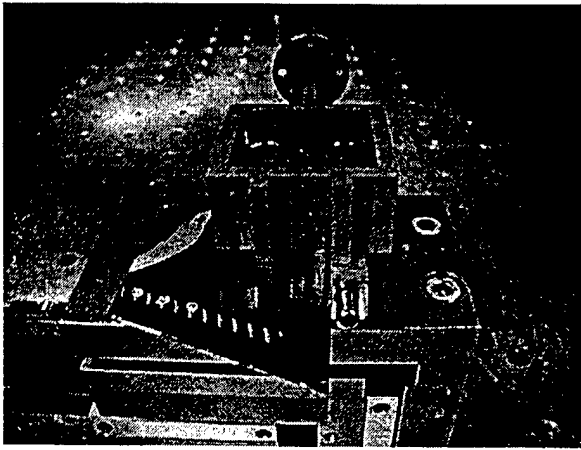
B. Tsap was with the Department of Electrical Engineering, University of California, Los Angeles, CA 90095 USA. He is now with Pacific Wave Industries, Los Angeles, CA 90024 USA.

A. Chen, S.-S. Lee, J. Chen, W. H. Steier, and L. R. Dalton are with the Department of Electrical Engineering and Chemistry, University of Southern California, Los Angeles, CA 90089 USA.

Publisher Item Identifier S 1041-1135(99)00339-0.



(a)



(b)

Fig. 2. (a) Photograph of the fabricated polymer modulator with integrated finline transitions at both ends of the traveling-wave electrode. (b) Photograph of the packaged W-band polymer modulator. This shows one modulator in the array connected to the rectangular waveguide.

A thick photoresist was patterned to define the top electrode and the upper finline transition. This pattern was precisely aligned to the polymer optical waveguide and the lower finline. Electrochemical gold plating was used to increase the thickness of the top electrode to $7\ \mu\text{m}$. The end surfaces of the optical waveguide were prepared using a dicing saw. A photograph of the fabricated device is shown in Fig. 2(a). The particular finline transition region to be inserted into the rectangular waveguide was separated from the array and the polymer layers on the lower finline transition pattern removed using a solvent. The transition was then inserted into the waveguide as shown in Fig. 2(b).

Previously, we have made polymer modulator devices using PUR-DR 19 that had an electrooptic coefficient $r_{33} = 15\ \text{pm/V}$, about half that of LiNbO_3 . Recent efforts in nonlinear organic chemistry have resulted in the synthesis of polymers with electrooptic coefficients close to or even exceeding that of LiNbO_3 . This is a direct consequence arising out of a better understanding of the London forces governing the dipole-dipole electrostatic interactions [6]. One such polymer developed by Dalton *et al.* is amino phenylene isophorone isoxazalone (APII) which has a $r_{33} = 30\ \text{pm/V}$ at an optical wavelength of $1.06\ \mu\text{m}$ [1]. In addition to impressive nonlinearities, APII has exhibited low optical losses and high stability. Fig. 3 shows the

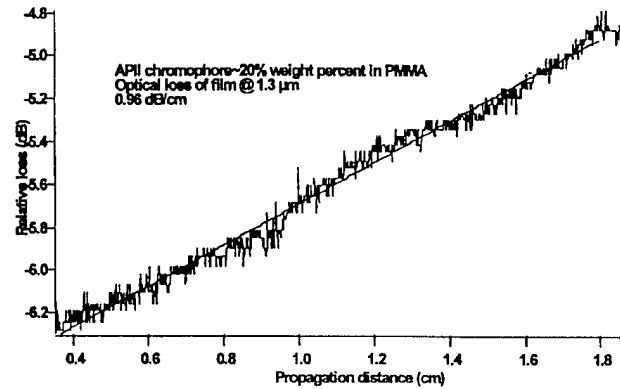


Fig. 3. Optical loss of the APII as a function of the propagating distance. Note that losses typically increase after crosslinking.

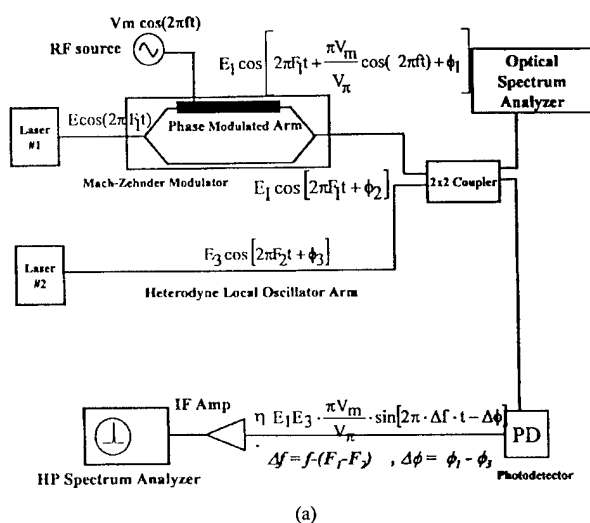
intrinsic optical loss ($\sim 1\ \text{dB/cm}$) of the APII as a function of the propagating distance of light. The temporal stability of the induced acentric dipole alignment is achieved by incorporating chromophores into a crosslinked polyurethane thermosetting network. This increases the optical losses slightly, but makes these systems very robust. We have used them with relatively high-power levels ($>20\ \text{mW}$) for long periods of time. APII exhibits high thermal stability, the decomposition temperature being $235\ ^\circ\text{C}$. Alignment temporal stability ranges from $90\ ^\circ\text{C}$ to $120\ ^\circ\text{C}$ for a crosslinked polymer network.

The performance of these APII polymer devices was measured using an optical heterodyne technique [7]. This technique involves mixing of the modulated output of our device and the output of a tunable laser that is set at a fixed frequency away from the center frequency of the modulated laser beam. A generalized schematic of this measurement is shown in Fig. 4(a). Assuming small-signal case, one of the terms generated by the beating between the three arms has a frequency $\Delta f = f - (F_1 - F_2)$ and has the following form:

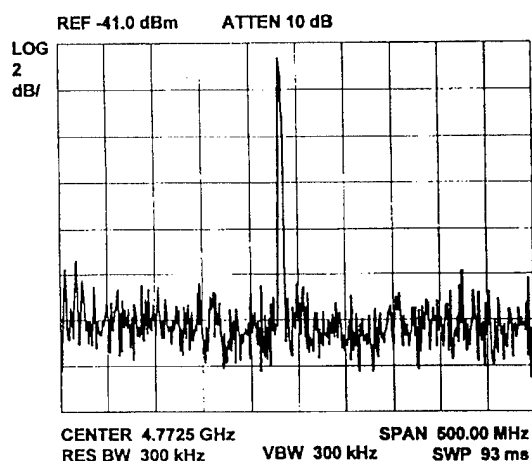
$$E_1 E_3 \cdot \frac{\pi V_m}{V_\pi} \cdot \sin[2\pi \cdot \Delta f \cdot t - \Delta\phi] \quad (1)$$

where E_1 and E_3 are electric field strengths in the first and third arm, respectively, V_m and f are the peak voltage and frequency of the microwave signal, $F_1 - F_2$ and $\Delta\phi = \phi_1 - \phi_3$ are the difference in frequency and static phase between the two lasers and V_π is the half-wave voltage of the phase modulator. By tuning the two lasers, Δf can be made to fall in the IF band of our detection setup. The magnitude of the photocurrent generated by the detector is inversely proportional to the V_π of the modulator at the frequency of operation. Since it depends only on the interaction between the phase-modulated arm and the heterodyne arm, this technique can be used equivalently to measure the frequency performance of phase and Mach-Zehnder modulators.

Light from a diode-pumped Nd:YAG laser ($\lambda = 1310\ \text{nm}$) was butt-coupled to the optical waveguide endface of our modulator using a single-mode PM fiber. Light for the local oscillator was derived from an external-cavity semiconductor diode laser, which could be tuned several hundreds of gigahertz around the Nd:YAG laser. Fine tuning of the difference frequency was achieved by precisely adjusting the frequency



(a)



(b)

Fig. 4. (a) Generalized schematic of the optical heterodyne setup showing the Mach-Zehnder structure and local oscillator configuration. (b) Modulation signal of the APII phase modulator at 95 GHz down-converted to an IF of 4.77 GHz.

of the Nd:YAG laser. Both beams were combined using a 2×2 fiber beam splitter and made incident on a photodetector. A 50-mW GUNN diode was used as the microwave source at 95 GHz. The spectrum analyzer trace of the downconverted signal at 95 GHz for the APII integrated phase modulator is shown in Fig. 4(b). This is an encouraging result for a phase modulator that has a $V_\pi = 16$ V, that corresponds to a V_π of 10.6 and 5.3 V in Mach-Zehnder and push-pull configurations, respectively.

To test the performance of the APII based modulators to 40 GHz, we fabricated a set of Mach-Zehnder devices on silicon substrates. The major fabrication steps were similar to those outlined for the devices on Mylar substrates. For an electrode-waveguide interaction length of 1.7 cm, the V_π of these devices in a Mach-Zehnder configuration was 10 V. In a push-pull configuration, this would correspond to a $V_\pi = 5$ V, which makes this new set of polymer devices acceptable for commercial applications. Two tunable diode pumped Nd:YAG lasers at $1.319 \mu\text{m}$ were used as sources for lower frequency

optical heterodyne measurement of the modulation signal. The initial measurements on the modulator showed considerable rolloff over the 0–40-GHz band of operation resulting from losses in the microstrip line. As we have found in related polymer structures, the V_π can be made almost flat over this frequency range by increasing the thickness of the microstrip line.

Traditionally, it has been accepted that the main advantage of polymer modulators over LiNbO₃ modulators is their ultrahigh-theoretical bandwidth. This results from the polymers' almost perfect velocity match that allows them to be configured as traveling-wave devices [8]. However, the problem of the limited nonlinearities in polymer materials has so far kept them from finding widespread use. This new generation of polymer devices have shown vast improvement in performance over DR19 [9] and can compete with LiNbO₃ devices in many important applications.

In conclusion, APII, a new polymer material with high nonlinearity and low optical loss has been synthesized and used to fabricate arrays of ultrahigh-frequency phase modulators with integrated finline transitions. These modulators have been tested at 95 GHz. The excellent microwave performance of the integrated transition signals the first successful efforts in packaging of polymer modulators at such high frequencies. Using this new polymer, Mach-Zehnder modulators have been fabricated and shown to work over a wide frequency band. Both these devices have shown very low V_π and have the ability to be commercially fabricated and packaged. Hence, these devices have widespread potential applications in commercial communication and military systems.

REFERENCES

- [1] J. Chen, J. Zhu, A. Harper, F. Wang, M. He, S. Mao, and L. R. Dalton, "Synthesis and characterization of a high- $\mu\beta$ chromophore containing the isophorone moiety for electro-optic applications," *Polymer Preprints*, vol. 38, no. 2, pp. 215–216, 1997.
- [2] K. W. Beeson, P. M. Ferm, K. A. Horn, C. W. Knapp, M. J. McFarland, A. Nahata, J. Shan, C. Wu, and J. T. Yardley, "Polymeric electro-optic materials and devices: Meeting the challenges of practical applications," *Nonlinear Optical Properties of Organic Materials VI, Proc. SPIE*, 1993, vol. 2025, pp. 488–498.
- [3] *Polymers for Second-Order Nonlinear Optics*, G. A. Lindsay and K. D. Singer, Eds. Washington DC: Amer. Chem. Soc., 1994.
- [4] Y. Shi, W. H. Steier, L. Yu, M. Chen, and L. R. Dalton, "Large stable photoinduced refractive index change in a nonlinear optical polyester polymer with disperse red side groups," *Appl. Phys. Lett.*, vol. 58, no. 11, pp. 1131–1133, Mar. 1991.
- [5] D. Chen, H. R. Fetterman, A. Chen, W. H. Steier, L. R. Dalton, W. Wang, and Y. Shi, "Demonstration of 110 GHz electro-optic polymer modulators," *Appl. Phys. Lett.*, vol. 70, no. 25, pp. 3335–3337, June 1997.
- [6] L. R. Dalton, A. W. Harper, and B. H. Robinson, "The role of London forces in defining noncentrosymmetric order of high dipole moment-high hyperpolarizability chromophores in electrically poled polymeric thin films," *Proc. Nat. Acad. Sci. USA*, vol. 94, pp. 4842–4847, May 1997.
- [7] W. Wang, D. Chen, H. R. Fetterman, Y. Shi, W. H. Steier, and L. R. Dalton, "Optical heterodyne detection of 60 GHz electro-optic modulation from polymer waveguide modulators," *Appl. Phys. Lett.*, vol. 67, no. 13, pp. 1806–1808, Sept. 1995.
- [8] R. Lytel, "Applications of electro-optic polymers to integrated optics," in *Nonlinear Optical Materials and Devices for Photonic Switching, Proc. SPIE*, Jan. 1990, vol. 1216, pp. 30–40.
- [9] W. Wang, D. Chen, H. R. Fetterman, Y. Shi, W. H. Steier, and L. R. Dalton, "Traveling wave electro-optic phase modulator using cross-linked nonlinear optical polymer," *Appl. Phys. Lett.*, vol. 65, no. 8, pp. 929–931, Aug. 1994.